Influence of regular surface waves on the propagation of gravity currents: experimental and numerical modeling

Rosaria E. Musumeci [1]; Antonino Viviano [2]; Enrico Foti [3]

ABSTRACT

The propagation of gravity currents is analyzed in the presence of regular surface waves, both experimentally and numerically, by using a full-depth lock-exchange configuration. Full-depth lock-exchange releases have been reproduced in a wave flume, both in the absence and in the presence of regular waves, considering two fluids having densities ρ_0 and ρ_1, with $\rho_0 < \rho_1$. Boussinesq gravity currents have been considered here ($\rho_0/\rho_1 \sim 1$), with values of the reduced gravity g' in the range $0.01 \div 0.1$ m/s^2, while monochromatic waves have been generated in intermediate water depth. The experimental results show that the hydrodynamics of the density current is significantly affected by the presence of the wave motion. In particular, the front shows a pulsating behavior, the shape of the front itself is less steep than in the absence of waves, while turbulence at the interface between the two fluids is damped out. In the present test conditions, the average velocity of the advancing front may be decreased in the presence of the combined flow, as a function of the relative importance of buoyancy compared to wave-induced Stokes-drift. Moreover, a new numerical model is proposed, aiming at obtaining a simple, efficient and accurate tool to simulate the combined motion of gravity currents and surface waves. The model is derived by assuming that surface waves are not affected by gravity current propagation at leading order and that the total velocity field is the sum of velocities forced by the orbital motion and those

[1]Assistant Professor, Dept. Civil Engineering and Architecture, University of Catania, Via S. Sofia 64, Catania 95123, Italy (corresponding author). Email: rmusume@dica.unict.it.

[2]Postdoctoral Researcher, Dept. Civil Engineering and Architecture, University of Catania, Via S. Sofia 64, Catania 95123, Italy. Email: antonino.viviano@dica.unict.it.

[3]Professor, Dept. Civil Engineering and Architecture, University of Catania, Via S. Sofia 64, Catania 95123, Italy. Email: efoti@dica.unict.it.

forced by buoyancy. A Boussinesq-type wave model for nonstratified fluids is solved, and its results are used as input of a gravity current model for stratified flows. Comparisons of the numerical results with the present experimental data demonstrate the capability of the model to predict the main features of the analyzed phenomena concerning propagation of the density current (averaged velocities, front height, etc.), the increase of entrainment of the ambient fluid into the density current in the presence of the waves and the intra-wave pulsating movement of the heavy front.

Keywords: gravity currents, waves, lock exchange, numerical model, experiments.

INTRODUCTION

Gravity currents are quite common both in natural, urban or industrial environments. They occur when a fluid flows in a fluid with a different density. For example, river discharges or outflows from industrial plants (e.g. cooling waters, brines, etc.) belong to this type of flows. In coastal environments, the dynamics of buoyancy-driven flows may be importantly influenced by the presence of tides and wind waves. A classical example is the propagation of the salt wedge within estuaries (Wright et al. 1988; Wright et al. 2001).

In the literature the dynamics of gravity currents has been widely investigated, often by considering the well-known lock-exchange problem (e.g. Benjamin 1968; Turner 1973; Ungarish 2009). In a classical lock-exchange problem, two zones with liquids having different densities, ρ_0 and ρ_1 with $\rho_1 > \rho_0$, are initially at rest, separated by a gate. In full-depth lock-exchange, the heavier fluid on one side and the lighter fluid on the other side occupy the entire water column h before the gate is removed. Once the lock is open, the positive front of the heavier fluid propagates close to the bottom with a velocity U, and the negative front of lighter fluid propagates in the opposite direction, close to the surface.

Several lock-exchange problems have been extensively investigated both analytically, experimentally and numerically, such as full-depth and partial depth two-dimensional cases (Huppert and Simpson 1980; Shin et al. 2004), axisymmetric cases or three-dimensional gravity currents over both smooth and rough bottoms (La Rocca et al. 2008). Furthermore,

Theiler and Franca (2016) analyzed the influence of the released volume in full-depth lock-exchange experiments, obtaining that density currents with high volume of release conserved the energy during their propagation.

Notwithstanding the fact that the development of gravity currents in the sea is frequent, the effect of the wave motion on the propagation of buoyancy-driven flows has been much less investigated and only few seminal work exists (Ng and Fu 2002; Robinson et al. 2013). Ng and Fu (2002) developed an asymptotic theory to study the effect of partially standing free-surface water waves on the spreading of a thin dense viscous gravity current, proving that a stratified wave boundary layer differs in a non trivial manner from a homogenous one. Indeed, under the assumptions that the dense liquid layer thickness was the same order of the Stokes wave boundary layer thickness and of the magnitude of the wave amplitude, they found that the wave-induced streaming current accelerates the flow of the fore front of the dense liquid and at the same time it decelerates the offshore-directed front of the density current. As a consequence, they observed a migration of the current in the direction of wave propagation, with fore fronts steeper compared to the case without waves, and also steeper than the offshore-directed fronts. Finally they suggested that wave streaming dominates over buoyancy in shallow waters, whereas the opposite occurs in deep waters.

More recently, Robinson et al. (2013) have investigated experimentally the effects of wave motion on gravity currents and they have shown that the presence of an oscillatory motion may influence significantly gravity current hydrodynamics. The gravity current flow was generated by releasing a finite volume of saline solution into a tank with an established periodic wave field. The front of the gravity current oscillated with amplitude and phase that correlated with the orbital velocities. The position of the gravity current centre and the shape of the two fronts, one propagating in the wave direction and one against it, were found to be significantly affected by the wave action. For long waves, the centre was advected downstream in the direction of wave propagation owing to the dominance of the Stokes drift. For short waves, the gravity current centre moved upstream against the wave direction, since

under these wave conditions the Stokes drift is negligible at the bed.

The aim of the present contribution is to investigate how buoyancy-driven gravity currents are modified by surface regular gravity waves, focusing on the nearshore region, where discharges of fresh, brackish or brine waters are usually located. Either due to the small density differences or to the discharge dynamics itself, such discharges may occupy a significant portion of the water depth, showing substantial differences with spill processes in the ocean, as the ones analyzed by Ng and Fu (2002). In engineering applications the problem is relevant, since in the shallow water depths which characterizes estuaries and nearshore regions, the wave-induced oscillating motion penetrates along the water column down to the bottom, thus potentially affecting the dynamics of the propagating density current and its capacity of transporting materials such as contaminants or sediments.

An objective of the present work is to characterize the hydrodynamic of the gravity current in the presence of waves, particularly in terms of velocity of the gravity current front. Ng and Fu (2002) and Robinson et al. (2013) focused on spills of high density and/or high viscousity fluids. Notwithstanding the light shed by these pioneering studies, their results can be hardly compared with the large amount of previous literature results on gravity current dynamics. Such results have been obtained using lock-exchange configurations, by means of analytical approaches (Benjamin 1968; Ungarish 2007), experimental methods (Huppert and Simpson 1980; Shin et al. 2004; La Rocca et al. 2008) and numerical models(Härtel et al. 2000b; Härtel et al. 2000a; La Rocca et al. 2012).

For this reason, the authors decided to use a lock-exchange schematization, where a surface wave field, characterized by height H_w and wave period T_w, is superimposed to the gravity current. The chosen approach allows to investigate the front dynamics in details, since, just after the fast initial transient, the average front velocity becomes constant, leading to a steady-state condition. Such a combined flow has never been studied before, to the authors' knowledge.

In the present work the problem has been tackled both experimentally and numerically.

In particular: (i) a laboratory study has been carried out in a wave flume to investigate the classical full-depth lock exchange release, also in the presence of regular monochromatic waves; (ii) a new gravity current numerical model has been developed and validated by using the present experimental data on the propagation of the front of the heavy fluid, e.g. the. gravity current head.

The experimental investigation is focused on the estimate of the average velocity of the front of the gravity current. To this aim, lock-exchange tests with similar values of the water depth and of the reduced gravity $g' = g(\rho_1 - \rho_0)/\rho_0$ have been carried out both in the absence and in the presence of a regular wave motion in intermediate depth conditions. It will be shown that the presence of the waves induces a modification of the way the gravity current propagates, by causing oscillation of the front, a reduction of the Froude number of the gravity current F, which represents the ratio between the average front velocity U and the initial buoyancy velocity $u_b = \sqrt{g'h}$, as well as by affecting the turbulence of the flow.

Concerning the numerical model, it should be mentioned that in the past gravity currents have been widely investigated by using different kinds of Computational Fluid Dynamics (CFD) models, either simplified shallow water models (see e.g. Ungarish 2009; La Rocca et al. 2012) or more complex Large Eddy Simulation (LES) (Ooi et al. 2007; Ooi et al. 2009) or Direct Numerical Simulation (DNS) models (Härtel et al. 2000b; Härtel et al. 2000a). The shallow water models assume steep fronts, well stratified flows and usually no entrainment of ambient fluid into the gravity current and they are able to catch just the main features of the complex flow dynamics. Some attempt has been done also to include entrainment in this type of models, by introducing a simple linear term in the equation of mass conservation (Ross et al. 2006; Adduce et al. 2012; Johnson and Hogg 2013). On the other hand, LES and DNS models allow to accurately resolve the vortical structures of the flow and the related dissipation, but they are computationally very expensive.

In the above framework, trying to fill the gap between the two mentioned approaches, a new computationally efficient two-dimensional numerical model is proposed for investigating

the combined wave-gravity current flow, including the non-homogenous density distribution along the water column. Under the assumption that at leading order the effects of buoyancy on the wave propagation can be neglected, the model decouples the total velocity field into a wave-component and a buoyancy-driven component. The latter one is calculated based on the first one, through the pressure term. Comparison of the numerical results of the model with the present experimental data allows to highlight its good prediction capabilities both in quiescient ambient fluid and in the presence of the combined wave and buoyancy-driven flow and its ability to provide a fair description of the density field. In particular, results on the entrainment are also presented.

The work is organized as follows. The following section describes the experimental set-up and laboratory results. Then, the governing equations of the proposed numerical model are derived and the performances of the model are discussed by comparing with the present experimental data and an established literature model. Finally, entrainment is analyzed in terms of numerical results. The main conclusions of the work are summarized in the last section.

EXPERIMENTAL SET-UP AND PROCEDURE

The experiments were carried out at the Hydraulic Laboratory of the University of Catania, within a wave flume which is 9m long, 0.5m wide and 0.7m high. The flume is equipped with an electronically-controlled oleodynamic piston-type wavemaker.

The lock is created by a Perspex sluice gate, located $5.15m$ far from the wavemaker. The same water depth is imposed at the two sides of the gate. The position of the sluice gate has been chosen in such a way that evanescent modes (i.e. surface waves that only exist near the wavemaker) vanish before the waves reach the gate (Dean and Dalrymple 1991). In this way fully developed waves interact with the gravity current propagation. The lock length of the gravity current x_0 was kept constant for all the experiments and was equal to 5.5m. Such a value takes into account the presence of the volume of water, offshore of the wave paddle (see Figure 1), which is necessary for wave generation. At the end of the flume

a porous beach allows to minimize wave reflection.

In order to reproduce a set-up schematically similar to the classical lock-exchange problem and to have at the same time a realistic representation of the physics, salt water, having density ρ_1, is present at the wavemaker side of the gate, and fresh water, having density $\rho_0 < \rho_1$, at the onshore side (see Figure 1). This situation is an idealization of real coastal environments where surface waves are generated offshore in a denser fluid and propagate toward regions where lighter waters are present (e.g. estuaries or industrial discharges).

To obtain different densities, tap water is mixed with sodium chloride (NaCl). Moreover, a diluted green dust organic food dye, combination of E102, E131, E514, is used to highlight the gravity current. The volume of salted water in the lock is about 0.5m^3. The concentration of the diluted dye is about 0.004%, thus differential diffusive effects between the brine and the dye are negligible.

Before starting each experiment, samples of the colored salt water and of the fresh water were gathered to measure the actual densities, ρ_1 and ρ_0 of the two fluids respectively. The densities of both the salted colored water and of the fresh water have been determined for each test by measuring their masses and by comparing them with that of the same volume of distilled water. To this aim, a set of three calibrated 100 ml picnometers, equipped with a thermometer having a precision of $0.005°C$, has been used. The mass of the fluids was measured by using a high precision scale (0.0001 g accuracy). By following the above procedure, the error in measuring the density is estimated to be smaller than 1 g/m^3.

Full-depth two-dimensional lock-exchange experiments have been carried out without and with superimposed surface regular waves.

In the first case, starting from an hydrostatic condition, the sluice gate is removed and a positive front of denser fluid intrudes in the lower part of the water column within the lighter fluid in the onshore direction while in the upper part a negative front of lighter fluid moves offshore.

In the second case, again starting from hydrostatic conditions, the wavemaker generates

a train of monochromatic waves which propagates in the onshore direction. As soon as the first wave crest is about to hit the gate, i.e. about 5.7 s after the wavemaker starts according to the present wave characteristics, the gate itself is manually removed. The removal takes about 0.3 s, while the wave period is about 1 s. It should be noted that the wave crest is the point which can be determined with the highest precision along the wave profile $O(4cm)$. The above experimental procedure guarantees that the removal of the gate is performed in such a way that wave reflection from the gate does not affect the wave train which interacts with the gravity current.

Thanks to the small scale apparatus, wave generation within the flume is highly repeatable. Additional experiments in the presence of a homogeneous density fluid (i.e. just fresh or salted water) have been carried out in order to measure the wave characteristics by means of resistive wave gauges installed at the gate location. This was deemed necessary since resistive gauges cannot be used if the salinity changes along the water column, i.e. during gravity current propagation. This procedure is possible thanks to the Boussinesq approximation used here, which allows to assume that the effect of the density on the wave generation is negligible. Such an assumption has been also verified experimentally by using acoustic wave gauges. In order to estimate the order of magnitude of the wave-induced mass transport, in the absence of the gravity current, a Nortek Vectrino Profiler has been used to obtain the time-average three-component velocity profile along the water column. This is obtained by a mosaic of individual velocity profiles each one measured over a vertical range of 3 cm, with a spatial resolution of 1 mm and a sampling rate of 100 Hz.

A Sony HDR-PJ10/EB camera recorded the propagation of the gravity current at a frame rate of 50 fps, with images which are 1920×1080 pixel wide leading to a spatial resolution of 0.71 mm x 0.53 mm. Great care has been used when positioning the camera in front of the measuring area. The parallelism of the image plane and of the side wall of the flume, where measurements of the front are gathered, has been carefully checked, as well as the minimization of lens distortion. A 10 cm by 10 cm grid on the glass wall of the flume helped

the metric calibration of the images.

A simple automatic procedure was implemented to analyze the recorded images, to recover the shape front of the gravity current and to calculate the front velocity and front height.

Preliminarily, it has been checked that the camera had a linear transfer function between light absorbance and concentration of the colored salt water, as suggested by Kolar et al. (2009) and by Nogueira et al. (2013).

For each experiment the recorded high resolution video sampled at 50 frames per second are treated to grab single snapshots as color RGB images, which are thus converted into gray scale images. Then, the measuring region between the sluice gate and a section about 40 cm downstream of the sluice gate itself is isolated into the images (see Fig. 2a).

The initial frame is considered as a reference frame. The intensity I_0^i of i-th pixel of the above grayscale reference frame is subtracted from the intensity of the corresponding pixel of each subsequent n-th frame I_n^i in order to obtain an enhanced image with intensities

$$\hat{I}_n^i = I_n^i - I_0^i \tag{1}$$

with $n = 1, 2, \ldots, N$, and N the total number of analyzed frames.

By following such a procedure, the resulting image (see Fig. 2b) highlights the dynamics of the front, since all the pixels of the enhanced image share the same reference level of light intensity and background disturbances are automatically removed.

To facilitate the measure of the front characteristics, the grayscale images were converted into binary black and white images (see Fig. 2c), by using a threshold on the pixel intensity, whose value has been determined through a sensitivity analysis. The front location was determined simply by counting the number of black pixels at the bottom along the horizontal direction, while the shape of the front is recovered as the interface between the black and white regions. By following the above procedure, it is estimated that the errors on the

location of the front of the gravity current is smaller than 0.5 mm.

Figure 2 shows an example of the outcome of the adopted image processing.

EXPERIMENTAL RESULTS

Table 1 reports the control parameters of the experiments, in particular the first column indicates the name of the test, where the prefix S refers to classical lock-exchange tests while the prefix W indicates that density currents and surface regular waves have been combined. The second column reports the water depth h, the third column shows the initial aspect ratio R, defined as the ratio between the initial depth of the current h and the initial length of the lock x_0 ($R = h/x_0$), which is in the range $0.026 \div 0.036$. Such values are smaller than those usually presented in the literature. For example in their experiments Huppert and Simpson (1980) use aspect ratio one order of magnitude or more larger than the present ones (e.g. $R = 0.126 \div 1.475$). According Shin et al. (2004), such small values of R avoid effects of the finite length lock on the current, guaranteeing at the same time the persistence of a slumping stage throughout the experiment. Moreover, the long lock length, and consequently the small value of R of the present experiments, was required to avoid effects of evanescent modes and undesired wave reflection from the lock gate. The fourth and the fifth columns give the densities of the light and of the heavy fluids, ρ_0 and ρ_1 respectively. The sixth column indicates the dimensionless density $\gamma = \rho_0/\rho_1$, which is always close to 1, since only Boussinesq currents have been considered here. The seventh column presents the reduced gravity $g' = g(\rho_1 - \rho_0)/\rho_0$, which is in the range $0.010 \div 0.172$ m/s^2. In the case of regular wave experiments the eighth and the ninth columns report the measured wave height H_w and wave period T_w, which were kept constant during the present experimental study. In particular, the data on H_w and T_w confirm the high repeatability of the wave experiments within the present apparatus.

In Table 1, tests having the same number correspond to similar gravity current conditions, carried out in the absence and in the presence of surface waves. An analysis of the correspondence between such tests is reported in Table 2, which shows for each couple of

experiments, the absolute relative errors $e_{g'}$, e_{ub} ad e_{Tc} calculated in terms of the reduced gravity g', initial buoyancy velocity $u_b = \sqrt{g'h}$ and of the time scale $T_c = h/u_b$ respectively. The results show that although g' may be different in some of the coupled tests, errors are systematically smaller when looking at the errors in terms of u_b and T_c. In particular, e_{ub} is smaller than 25%, which is reasonable considering the large volumes $O(0.5\text{m}^3)$ of salted water at play.

In the absence of waves, the average velocity of the fore front U is calculated as the slope of the linear function which best-fit the experimental measurements of the x-position of the front in time. This is possible, since the current is observed during the constant speed-phase. In principle, such a constant-velocity phase should be reached briefly after the initial acceleration stage due to the gate opening. However, due to inertial effects and the manual opening of the lock, some disturbances can occur, which may delay the initiation of the slumping phase. In order to overcome such a problem, the actual instant t_{0s} of the starting of the constant-speed phase has been determined for each experiment and the linear regression has been calculated only by considering the data acquired for $t > t_{0s}$. Figure 3 shows for tests S001-S009 the dimensionless front propagation x_f/x_0 as a function of the dimensionless time t/t_0, with x_f being the distance of the fore front from the gate, and $t_0 = x_0/\sqrt{g'h}$ being the time scale. In particular, the Figure distinguishes the two datasets of the front position before and after t_{0s}, by reporting also the value of t_{0s} and the linear function used to estimate the average front velocity U. For some tests the duration of initial transient may be significant, particularly for the tests where the reduced gravity is very small (e.g. S001-S006), since inertia prevails on buoyancy effects. If the reduced gravity is larger, as in tests S007-S009, the initial transient is much smaller.

Analogously, Figure 4 shows the results obtained for the tests W001-W009, with superimposed regular surface waves. In this case, the front oscillates while propagating onshore, with the same frequency of the waves. Moreover, by following the procedure described above, the estimate of U is not affected by the oscillation of the front position due to the orbital

motion, and in turn by the actual phase of the waves. Finally, it may be noticed that when waves are superimposed to the gravity current, in general, t_{0s} is smaller than in the absence of waves, since inertial effects are overridden by the orbital motion.

Table 3 summarizes the measured average front velocity U and the kinematic and dynamic dimensionless parameters of the performed experiments, namely: the Froude number $F = U/u_b$; the Reynolds number $Re = Uh/\nu$, where ν is the kinematic viscosity of the water; the relative water depth kh and the wave steepness ka, with $a = H_w/2$ being the wave amplitude. The wave number $k = 2\pi/L$, where L is the wavelength of the generated waves, is calculated by means of the linear dispersion relationship (Dean and Dalrymple 1991). The analysis of the values in Table 3 helps to characterize the conditions of the present experimental research.

In particular, in the absence of waves, the Froude number F is close to the theoretical value $F = 0.5$ predicted by the energy-conserving theory of Benjamin (1968) and confirmed experimentally by Lowe et al. (2005) and by Shin et al. (2004), and numerically by Härtel et al. (2000b). In the presence of waves F may be reduced up to 50%, particularly for smaller values of the buoyancy velocity, as shown also in Figure 8.

The Reynolds number $Re = Uh/\nu$ is in the range $1566 \div 18780$. Since $Re > 1000$, viscous effects on the density current propagation should be negligible (Simpson 1997). This is also confirmed by the results shown in Figures 3-4, where dissipation does not play a significant role.

The values of the relative water depth kh indicates intermediate water depth conditions, therefore the orbital wave motion interacts with the propagation of the gravity current over the entire water depth.

The small values of the wave steepness ka confirms that linear waves have been generated. Wave reflection in the flume has been measured by means of the two-gauge method proposed by Goda and Suzuki (1976). In all the tests the reflection coefficient is smaller than 15%, therefore almost purely progressive waves have been obtained, similar to the ones in the

nearshore region, in the presence of gravel or sandy beaches.

In order to preliminarily validate the tests carried out in quiescient ambient fluid, Figure 5 illustrate on a log-log scale the evolution of the dimensionless front position for the tests S001-S009 . The comparison with the reference slope equal to one (see for example Marino et al. 2005; Ooi et al. 2009), is also reported in Figure 5, and it is quite satisfactory. The initial discrepancies of the data with the theoretical slope are caused by spurious effects due to the opening of the gate.

Figure 6 shows an example of the dynamics of the front propagation in a quiescient ambient fluid, where the only forcing is buoyancy. The grayscale image and the measured shape of the front are shown at time intervals of 2s, starting from t=9s after the removal of the gate. The gate is located at $x = 0$m.

In such a case, many of the characteristics of the classical lock-exchange phenomena during the slumping stage can be observed (Benjamin 1968; Shin et al. 2004). In particular the slope of salt wedge is steep $O(60^\circ)$, while the depth of the gravity current h_F behind the front is about half of the water depth, i.e. $h/2 = 0.1$ m. Finally the rate of advancement of the front is constant as predicted by Benjamin's energy-conserving theory (Benjamin 1968), with the Froude number being equal to $F = 0.539$.

The interface between the lighter and the denser fluid is unstable. Quasi two-dimensional Kelvin-Helmholtz (K-H) billows are generated at the front by the shear between the two fluids. Their dimensions in the nearby of the front are O(2-5 cm). These KH billows move opposite to the gravity currents, increase their dimensions and then break up behind the front, inducing the entrainment mechanism of the ambient fluid into the gravity current. At about one water depth upstream of the front, it may be noticed that the turbulent perturbations at the interface are characterized by smaller spatial scales O(1 mm) and are almost uniformly spaced.

Figure 7 shows a similar plot for the case of the salt wedge propagation in the presence of the wave motion. Comparing with the results shown in Figure 6, several differences may

be noticed. First of all, the front of the heavier fluid is characterized by a smaller depth, $h_F \sim 0.8$m, and also the front steepness is reduced to about 50°. Moreover, the relative rate of advancing of the front $F = U/u_b$ in the onshore direction is sligltly slower compared to the classical lock-exchange case, being $F = 0.507$.

The presence of the orbital wave motion interacts with the formation and evolution of K-H billows: larger scale structures structures can be observed in this case. The dimensions of such structures, $O(5$ cm), is related to the dimensions of the orbital trajectories induced by the wave motion at an elevation about half of the interface. Due to the presence of small amplitude waves, the orbital motion at the interface between the two fluid is characterized by the clockwise movement of the fluid around closed elliptical trajectories. It follows that the development and upstream movement of the counterclockwise rotating K-H billows is retarded by the wave action.

Moreover, by comparing the gravity current fronts in Figures 6- 7, it can be observed that instabilities along the front are smoothed out in the presence of waves. Such a phenomenon could be due to a re-laminarization of the flow in the boundary layer at the interface, induced by the superposition of the wave oscillating motion to the gravity current. A similar process has been observed experimentally by investigating the wall-boundary layer in the presence of current-wave interaction, both in pipe flows by Lodhal et al. (1998) and in open-channel flows by Musumeci et al. (2006), who observed damping of the turbulence of the current and reduction of the current wall shear stresses, compared to the only current reference value, when the wave boundary layer was in the laminar regime and the flow was wave-dominated. In the present case, the waves are in the laminar regime, being the wave Reynolds number $Re_w = O(500)$, while the combined gravity current-surface wave flow is wave-dominated, being the ratio between the phase speed of the waves and the velocity of the gravity current larger than one. Therefore, suppression of turbulence of the gravity current is also expected in the case of combined flow.

Figure 8 reports a comparison between the buoyancy velocity u_b and the average front

velocity U measured in the absence of waves (tests S001-S009) and in the presence of waves (tests W001-W009). The prediction of Benjamin (1968) in the absence of energy losses, i.e. $F = U/u_b = 0.5$ is also shown in the Figure. As expected, data from tests S001-S009 tends to collapse on such a line. In general, the interaction with the wave motion induces a decrease of the relative front velocity, i.e. of the Froude number F. In particular such a decrease is larger when the buoyancy velocity is smaller, while in the case of $u_b > 0.1$ m/s, i.e. for the g' larger than 1.00 m/s^2, there is no significant difference between the two cases.

It must be considered that in the case of the combined gravity current-wave motion, the average speed of the gravity current should be influenced by the integral wave mass transport. In general, such a mass transport is composed by the offshore directed Stokes drift, induced by the irrotational wave motion, and by the onshore Eulerian drift, or steady streaming, generated within the thin wave boundary layer. The first develops immediately and acts along the most of the water column, while the second one develops after vorticity has spread from the bottom boundary layer over the entire water column, (Mei et al. 2005), and it is concentrated in a thin layer close to the bottom.

In the present experiments, due to adopted lock exchange schematization, only the Stokes drift was present. Indeed, according to Mei et al. (2005) an estimate of the time necessary to develop the steady streaming component is about $O(5$ min), while the duration of the experiments was $O(10$s). This is confirmed by the data reported in Figure 9, which show the time-averaged only-wave velocity profile U_w measured by means of the Vectrino Profiler for different duration of wave generation, i.e. after about 10s, when the steady streaming has not developed yet (see Figure 9a), and after 60 min, when the steady streaming is fully developed (see Figure 9b). In both cases, the time-average is carried out considering time series about 120-150 wave cycle long. It follows that, in the present experimental conditions, the offshore directed Stokes drift is about 0.6 cm/s, which agrees with the prediction of classic literature models (Longuet-Higgins 1970; Dean and Dalrymple 1991).

It turns out that if g' is very small, the Stokes drift, which is directed opposite to the

heavy front propagation, plays a role in decreasing the speed of the current. On the other hand, if the gravity current becomes faster, the effect of the Stokes drift may be unimportant.

Robinson et al. (2006) analyzed the effects of wave action on the propagation of gravity currents generated by the instantaneous release of a dense fluid. They attributed the asymmetry of the current height and the modification of shape of the gravity current to the shear of the mean flow generated by the wave motion. In particular, it has been observed that the mean advection of the gravity current is positively or negatively affected by the Lagrangian velocity which develops in the boundary layer and whose sign depends on the wavelength. The results in the present experiments, carried out in the presence of relatively long waves, confirm the experimental findings of Robinson et al. (2013).

PROPOSED NUMERICAL APPROACH

A new numerical model has been developed for the analysis of the combined two-dimensional motion of gravity current and free surface waves. The governing equations are obtained under the assumption of Boussinesq gravity currents. The reference system is shown in Figure 10, where the two-dimensional Cartesian coordinate system (x, z) is located on the still water level, from which water depth h is measured. By using an approach similar to that of Ungarish (2009), the continuity equation, the two momentum Reynolds-Averaged equations and the density transport equation are:

$$\frac{\partial u}{\partial x} + \frac{\partial w}{\partial z} = 0 \tag{2}$$

$$\rho \frac{du}{dt} = -\frac{\partial p}{\partial x} + \frac{\partial}{\partial z}\left(\tau_{xz} + \tau'_{xz}\right) \tag{3}$$

$$\rho \frac{dw}{dt} = -\frac{\partial p}{\partial z} + \frac{\partial}{\partial x}\left(\tau_{xz} + \tau'_{xz}\right) - \rho g \tag{4}$$

$$\frac{d\rho}{dt} = \kappa \left(\frac{\partial^2 \rho}{\partial x^2} + \frac{\partial^2 \rho}{\partial z^2} \right) \tag{5}$$

where u and w are the horizontal and vertical components of the total velocity $\boldsymbol{u} \equiv (u, v)$; p is the total pressure; τ_{xz} and τ'_{xz} are the viscous and turbulent stresses respectively; ρ is the

local density; g is the gravity acceleration; κ is the diffusion coefficient of the species that constitutes the density variation, which is equal to zero in the case of immiscible fluids.

Modelling the surface wave motion in a lock-exchange release is a complex task, which, thanks to the adopted Boussinesq approximation i.e. $\gamma = \rho_0/\rho_1 \sim 1$, is tackled here by decoupling the homogeneous density wave motion and the gravity current propagation forced by actual density gradients.

The total velocity field $\boldsymbol{u}$ is obtained by linearly adding up the velocity field due to the wave motion $\boldsymbol{u_B}$ and the one due to the gravity current $\boldsymbol{u_d}$:

$$\boldsymbol{u} = \boldsymbol{u_B} + \boldsymbol{u_d} \tag{6}$$

In particular, $\boldsymbol{u_B}(x, z, t) \equiv (u_B, w_B)$ is calculated using a Boussinesq-type wave model for homogeneous flow. Indeed, here, at leading order, the influence of buoyancy on the surface wave propagation is neglected, i.e. $\boldsymbol{u_B} \ll \boldsymbol{u_d}$. Such an assumption is also confirmed by the present experimental data.

The gravity current velocity field $\boldsymbol{u_d}(x, z, t) \equiv (u_d, w_d)$ is established due to the variable density field $\rho(x, z, t)$, which is comprised in the range $\rho_o \div \rho_1$, and it is evaluated as a function of the pressure field induced both by buoyancy and by the waves.

Homogeneous flow under surface waves

In order to describe the hydrodynamics of surface waves, the one dimensional weakly-dispersive fully-nonlinear Boussinesq-type model of Musumeci et al. (2005) has been adopted here. Such a model was originally derived to describe surf zone hydrodynamics and it has been recently extended by Lo Re et al. (2012) and by Viviano et al. (2015) to deal with wave run up and current circulation in the nearshore area.

Coupled with the gravity current model which will be described in the following Section, such a model allows to investigate salt wedge propagation in the presence of waves in nearshore regions. This may be important in engineering applications, such as the study of

the dynamics of wastewater or industrial discharge along the coast. Some preliminary tests in the presence of breaking waves have been already presented in Viviano et al. (2014).

On the basis of scaling arguments for relatively shallow water waves propagation, two dimensionless parameters are adopted, namely the dispersive parameter $\mu = kh$ and the nonlinear parameter $\delta = a/h$. Being weakly dispersive, only terms up to $O(\mu^2)$ are retained, whereas being fully nonlinear no assumptions are made about the order of magnitude of δ.

In the original version of the model, it is assumed also that the flow is irrotational only outside of the surf zone, wave breaking being be the unique source of vorticity. Therefore, within the surf zone the velocity field is influenced by the effects of breaking-induced vorticity. The vorticity transport equation is solved analytically. The amount of vorticity introduced by the breaking process is determined through a similarity with the hydraulic jump, by using the surface roller concept (Svendsen et al. 1978).

The governing equations of the Boussinesq-type wave model have been derived by integrating the Reynolds equations over the depth and by applying the wave kinematic and dynamic boundary conditions at the bottom and at the free surface, i.e. : (i) the free slip condition has been considered at the impermeable and fixed bottom; at the free surface, (ii) the velocity is equal to the time derivative of free surface elevation and (iii) the relative pressure is null. The surface elevation, ζ, and the depth-averaged orbital velocity, $\overline{u}$, are used as dependent variables. The interested reader is referred to Musumeci et al. (2005) for details on the derivations.

Starting from the solution of the above model, it is possible to extract information on the horizontal component of the orbital flow motion u_B in non-stratified conditions:

$$u_B = \overline{u}_p + \mu^2 (h\overline{u}_p)_{xx} \left(\frac{\Delta_1}{2} - z \right) + \frac{\mu^2}{2} (\overline{u}_p)_{xx} \left(\frac{\Delta_2}{3} - z^2 \right) + u_r \tag{7}$$

where $\overline{u}_p$ is the depth averaged potential velocity, which coincides with the depth-averaged total orbital velocity $\overline{u}$ in the absence of breaking waves, since in this case the rotational

velocity u_r is null. Δ_1 and Δ_2 are coefficients given by the following expressions:

$$\Delta_1 = \delta\zeta - h\ , \quad \Delta_2 = \delta^2\zeta^2 - \delta\zeta h + h^2 \tag{8}$$

Once the horizontal component of orbital velocity u_B is obtained over the entire domain, the vertical component w_B can be derived numerically on the basis of the continuity equation, as follows:

$$\begin{aligned} w_B = \; & - \; (\overline{u}_p)_x(z+h) - 2\overline{u}_p h_x - \mu^2(h\overline{u}_p)_{xxx}\left[\frac{\Delta_1}{2}(z+h) - \frac{z^2}{2} + \frac{h^2}{2}\right] \\ & - \; \mu^2(h\overline{u}_p)_{xx}\left[\frac{(\Delta_1)_x}{2}(z+h) + 2hh_x + \Delta_1 h_X\right] \\ & - \; \frac{\mu^2}{2}(\overline{u}_p)_{xxx}\left[\frac{\Delta_2}{3}(z+h) - \frac{z^3}{3} - \frac{h^3}{3}\right] \\ & - \; \frac{\mu^2}{2}(\overline{u}_p)_{xx}\left[\frac{(\Delta_2)_x}{3}(z+h) - 2h^2h_x + \frac{2}{3}\Delta_2 h_x\right] \end{aligned} \tag{9}$$

Gravity current model for stratified flow

The velocity field and free surface elevation obtained through the above wave model represent the input variables of the gravity current model proposed here, which is a modified version of those proposed by Viviano et al. (2014) and by Viviano et al. (2016). In particular, here the turbulence model has been improved to better simulate the full depth lock exchange phenomenon.

The presence of a spatial variability of density influences the flow only through its effect on the pressure field. Thus the Reynolds Averaged Navier Stokes momentum equations, i.e. eqs. (3)-(4), can be rewritten in terms of a new pressure term related to stratification, called $p_d = p - p_0$, where p_0 is the pressure value in the case of non-stratified conditions. Considering the velocity decomposition introduced in eq. (6), the expression for the pressure can be obtained by subtracting the vertical component w_B obtained from eq. (9) from the

vertical momentum equation for the total vertical velocity w:

$$\rho\left(\frac{dw}{dt}+g\right)-\rho_0\left(\frac{dw_B}{dt}+g\right)=-\frac{\partial p_d}{\partial z}+\frac{\partial}{\partial x}\left[(\tau_{xz}+\tau'_{xz})-(\tau_{xz}+\tau'_{xz})_0\right] \tag{10}$$

The pressure term related to density variation can be calculated by integrating:

$$-\frac{\partial p_d}{\partial z}=\Delta\rho\left(\frac{dw}{dt}+g\right)+\rho_0\left(\frac{dw_d}{dt}\right)-\rho\frac{\partial}{\partial x}\left[(\nu+\nu_t)\left(\frac{\partial u_d}{\partial z}+\frac{\partial w_d}{\partial x}\right)\right] \tag{11}$$

in which $\Delta\rho=\rho-\rho_0$ is the local density variation with respect to the reference value ρ_0, and ν and ν_t represent the kinematic and the eddy viscosities respectively. The eddy viscosity is estimated on the basis of the formulation proposed by Smagorinsky (1964) for sub-grid scale turbulence, as a function of the local derivatives of the velocity field and the local grid size:

$$\nu_t=C\Delta x\Delta z\sqrt{\left(\frac{\partial u}{\partial x}\right)^2\left(\frac{\partial w}{\partial z}\right)^2+\frac{1}{2}\left(\frac{\partial u}{\partial z}+\frac{\partial w}{\partial x}\right)^2} \tag{12}$$

where C is a constant which has been considered equal to 0.004; Δx and Δz are the dimension of the numerical grid in the horizontal and in the vertical directions, respectively. The value adopted for the constant C in the turbulence model is similar to that used by Deardorff (1970) and Piomelli et al. (1988) when modelling turbulent channel flow.

The pressure p_d is assumed equal to zero on the free surface ζ. Once p_d is estimated through integration of eq. (11), it can be inserted in the horizontal momentum:

$$\frac{\partial u_d}{\partial t}+\frac{1}{2}\frac{\partial u_d^2}{\partial x}+w_d\frac{\partial u_d}{\partial z}+\frac{1}{\rho}\frac{\partial p_d}{\partial x}-\frac{\partial}{\partial z}\left[(\nu+\nu_t)\left(\frac{\partial u_d}{\partial z}+\frac{\partial w_d}{\partial x}\right)\right]=0 \tag{13}$$

where a no slip boundary condition is used at the bottom. Since the wave motion has been already solved through the above Boussinesq model, the unknown dependent variables of the present problem are p_d, u_d, w_d and ρ. For a complete solution of the problem four equations must be solved. Since eqs. (11) and (13) have been already considered, two additional

equations are taken into account. The first one is the density transport equation for miscible fluids, i.e. eq. (5); the second one is the continuity equation of the gravity current, obtained by combining eqs. (2) and (6):

$$\frac{\partial u_d}{\partial x} + \frac{\partial w_d}{\partial z} = 0 \tag{14}$$

Moreover, in the adopted formulation the free surface elevation ζ should be the sum of the two contributions ζ_B and ζ_d, due respectively to waves and buoyancy, i.e. $\zeta = \zeta_B + \zeta_d$. Here it is assumed that at leading order the wave motion dominates and the contribution due to density variations is considered to be negligble, i.e. $\zeta_d \ll \zeta_B$. However, when integrating eq. (11) along the water column to obtain p_d, the contribution to the free surface elevation ζ_d must also be included and it can be obtained by integrating eq. (14) along the water column and by applying the well-known kinematic boundary conditions at the free surface and at the bottom:

$$\frac{\partial \zeta_d}{\partial t} + \frac{\partial}{\partial x} \int_{-h}^{\zeta} u_d \mathrm{d}z = 0 \tag{15}$$

Numerical integration

In analogy with the scheme adopted in the Boussinesq-type wave model, the time-stepping of eqs. (5)-(13)-(15) is numerically performed by applying the third-order predictor and fourth-order corrector Adams-Bashfortf-Multon scheme (Press et al. 1992). Such a scheme has been chosen for its good stability properties. The corrector step, which is accurate up to $O(\Delta t^4)$, is repeated until the relative error is smaller than a fixed quantity for the variables u_d, ρ and ζ_d. When the iterative method is completed, the remaining variables, i.e. p_d and w_d, can be computed by integration along the water column of eqs. (11) and (14), respectively.

It is worth to specify that, in the absence of waves, the gravity current formulation described here is still valid since it can be applied by considering orbital velocities and free surface elevation equal to zero over the entire domain.

An absorbing-generating boundary condition (see van Dongeren and Svendsen 1997) is

implemented at the offshore side. Such a condition allows both to propagate waves inside the domain and to absorb reflected waves exiting the domain. A sponge layer, about a wavelength long, is used in front of the vertical wall at the onshore end of the domain to absorb incident wave energy and to damp undesired wave reflection. In the model, the kinematic viscosity of water has been assumed equal to 10^{-6} m^2/s, while sodium chloride is dissolved into water, thus the diffusion coefficient assumes a value of $\kappa = 1.5 \times 10^{-9}$m^2/s.

COMPARISONS BETWEEN EXPERIMENTAL AND NUMERICAL RESULTS

The validation of the proposed numerical model for the simulation of gravity current propagation both in the presence and in the absence of waves has been performed through a comparison with the data of the present experimental study. The numerical domain has a rectangular shape and is 14 m long and 0.3 m high. The spatial resolution differs between horizontal and vertical direction, indeed the grid is made up of 281 numerical points in the x direction and 41 points along the z direction. Thus the resulting uniform space discretization, along horizontal and vertical direction respectively, is: $\Delta x = 50$ mm and $\Delta z = 7.5$ mm.

In order to reproduce the full-depth lock-exchange schematization, the initial condition is characterized by the presence of two regions of fluid having uniform density along the entire water column. The region with the highest density ρ_1 is located at the seaward side of the domain and the one with the lightest density ρ_0 at the onshore side. The separation between the two regions is located at the center of the computational domain. The water depth is the same at the two sides of the lock.

Figure 11 shows the comparison between the evolution of the gravity current in the laboratory flume and that simulated by the proposed numerical model both for the tests S007 and W007. The first test is a classical full depth lock-exchange, the second one is the same test carried out in the presence of a superimposed regular surface wave field. In both cases, the reduced gravity current is $g' = 0.047$ m/s^2.

The laboratory images allow to highlight the presence of an entrainment layer at the interfaces of the two fluids. Therefore the capabilities of the numerical model can be tested

to describe the density variability both in time and space.

In particular, the dimensionless density differences $\Delta\rho^*$ calculated by the model are defined as

$$\Delta\rho^* = \frac{\rho - \rho_0}{\rho_1 - \rho_0} \tag{16}$$

with ρ being the actual value of the computed density. In Figure 12 the isolines of $\Delta\rho^*$ are superimposed to the snapshots of the front. Such a representation permits to compare the measured and calculated propagation of the positive and negative fronts and the evolution of their shape, also by considering the variability of density across such fronts.

A fairly good agreement between experimental and modeled heavy front is obtained at the front, since the numerical model is able to catch the overall dynamics of the gravity current propagation, both in the absence and in the presence of the waves.

The position in time of the two fronts is similar (see Figure 11). Both in the lab and in the model, when the waves are present the front is slower. The shape of the gravity current is reasonably reproduced. Indeed, the formation of a characteristic lobe on the more advanced part of the current and of vortex structures at the interfaces between the two fluids, due to the presence of a shear layer, are caught by the proposed numerical approach. Moreover, both in the experimental data and in the numerical results, it may be observed that such a shear, which leads to entrainment of ambient fluid into the density current at the interface, is larger in the absence of the waves. The modeled shape of the interface is more irregular than the observed one, particularly in the absence of surface waves. Such a difference may be related to the simplified modeling of the actual entrainment processes at the interface, since the proposed model is not able to consider the breaking up of K-H billows. The overall shape of the front and particularly the interface is more accurately modeled in the presence of waves, since the oscillating motion reduces the development of K-H instabilities.

The main discrepancies can be observed during the initial stages, after the removal of the gate, whereas the simulated propagation of the front is quite similar to that observed in the lab. One of the possible reasons for such discrepancies is the different mechanisms

of gate opening, which is manual in the lab and instantaneous in the model. Moreover, probably because of the adopted scaling and of the chosen simple turbulence closure, the proposed model is more suited to reproduce the horizontal propagation of the front, rather than the initially vertical dam-break dynamics. A simple falling body approach is adopted to estimate the initial dam-break duration, at which the numerical model may not be accurate. Such a a duration is estimated by considering a falling height equal to the vertical distance between the centroids of the heavy fluid both at the initial time and at the end of the lock exchange, i.e. when the front heights are respectively equal to h and $h/2$ respectively. Thus the falling height is equal to $h/4$, the dam-break time is $\sqrt{2(h/4)/g'}$. Considering the present conditions, values of such a time are in the range $1 \div 3$ s, which agrees also with the data shown in Figure 3.

In order to analyze the dynamics of the entrainment zone, particularly close to the front, several values of $\Delta\rho^*$ have been used to represent the front region obtained from the numerical model. In particular three different values of $\Delta\rho^* = 1/2$; $1/4$ and $1/8$ have been considered, the latter value better representing the position of the front, the others allowing to estimate the dimension of the entrainment layer.

Figure 12 shows the comparison between the experimental data and the numerical results of the time evolution of the front position in the absence of surface waves. Four experimental tests have been numerically simulated, having the same geometrical configuration and reduced gravity which ranges between 0.021 and 0.113 m/s^2. The theoretical prediction of Benjamin (1968), obtained assuming energy conservation, is also reported in Figure 12. Such a theory states that the velocity and the height of the heavy front are equal to

$$U = \frac{1}{2}\sqrt{(1-\gamma)gh} \tag{17}$$

$$h_f = \frac{1}{2}h \tag{18}$$

It can be noticed that the proposed model is able to quite satisfactorily reproduce the

experimental data, while the theoretical model of Benjamin (1968) tends to overpredict both the experimental and the numerical front velocity, particularly for small values of g' (e.g. test S004).

Probably due to the shock due to the gate opening, both the experimental data and the model results show some oscillations at the initial stages, which may be related to the heads cycles identified in Nogueira et al. (2014), whose periodicity is similar to that observed here. Such oscillations are later damped out only in the experimental data. Their persistence in the numerical simulations indicates that the turbulent dissipation obtained by the simple turbulence model adopted here is lower than that of the laboratory test. Moreover, the amplitude of such oscillations seems not to be related to the value of the density difference $\Delta\rho^*$.

In the presence of surface waves superimposed to the gravity current, the comparison between the experimental data and the numerical results is again generally fairly good, as shown in Figure 13, and the model is generally able to catch the reduction of averaged velocity of the front due to the orbital motion.

Only for test W004, which corresponds to the lowest value of reduced gravity g' there is a mismatch. The physical meaning of such a different behaviour is that the gravity current is more influenced by external forces when the buoyancy is low. In particular, the presence of orbital velocity induced by surface waves significantly reduces the gravity current velocity for small g'. Such an effect is not caught by the proposed decoupled numerical model, which may be not suitable to treat cases with small initial density differences, as shown also in Figure 12. Figures 12a and 13a show that the front reproduced by the model is faster compared to the experimental data. Indeed, in such cases the level of turbulence introduced by the simple closure model is not sufficient to slow down the current. Nevertheless the values of reduced gravity at which the model fails are very small and may not be important in real applications. Indeed the effluents in the coastal zones are usually due to: aquifer discharges, treatment plants, rivers. In all these cases the minimum difference between ambient and effluent density

is about 0.4% and the minimum reduced gravity is close to 0.04 m/s^2 (Crossland et al. 2005).

An important consequence of the presence of surface wave is that the instantaneous velocity of the front may be significantly different from the average velocity U. Its maximum value is to 4 times larger, in the investigated conditions. This strongly influences the transport processess of materials triggered by gravity currents in nearshore regions.

Moreover, in both numerical and experimental data, shown in Figure 13, the front position oscillates with a period which matches that of surface waves. This occurs not only at the forefront ($\Delta\rho^* = 1/8$), but also in the region immediately upstream ($\Delta\rho^* = 1/2; 1/4$), indicating that the thickness of the entrainment layer periodically varies due to the waves. More in details, the amplitude of the wave-generated front oscillations is larger for smaller values of $\Delta\rho^*$.

In order to further analyze the above wave-induced gravity current front oscillations, Figure 14 reports the measured and calculated normalized spectral components of the front positions X/X_{peak}, obtained by removing the trend related to the current propagation.

The comparison confirms that the model is able to predict the overall dynamics of the combined wave-gravity current flow. Indeed, as expected, since the flow oscillations are due to waves, the highest peak occurs at the surface wave frequency, $f_w = 1/T_w$ both in the model and in the experimental data. Small differences may be attributed to the different spectral frequency discretization used when analyzing the two datasets. Furthermore, the model is able to catch the secondary peak which appears at frequency lower than f_w which may be be due to a long wave induced by the initial opening of the lock gate. Moreover, the width of the spectrum becomes larger as g' increases. This is probably due to the exchange of momentum at higher frequency induced by the larger gravity current velocities and to a more unstable shear layer between the heavy and the light fluid.

Figure 15 compares the measured and the calculated instantaneous dimensionless velocity $u^* = u_f/\sqrt{g'h}$, being u_f the instantaneous velocity of the front, which is obtained by determining the time derivative of front position x_f. Due to the interaction with the waves,

both in the experiments and in the model the velocities oscillates with the same dimensionless period of the waves $T_w^* = T_w\sqrt{g'h}/h$ and the general agreement with the actual values of the velocities of the front is fair, though the model tends to cut out positive and negative peaks. Besides the scatter recovered in the experimental data, such differences are smaller for larger values of g', i.e. when the gravity current dynamics prevails on the effects of the orbital motion.

From the above results, it turns out that the analyzed combined flow is characterized not only by the longer time scale of the gravity current propagation but also by the shorter time scale of wave oscillations. In order to discuss the dynamics of the heavy front during the wave cycle, Figure 16 compares the measured and calculated front shapes considering several phases during a single wave period. The phase is assumed to be equal to zero when the surface wave crest has reached the front position. The results are shown each $\pi/4$ of T_w. The crest location is evaluated visually, with an uncertainty of about $\pm\pi/16$.

Both the laboratory and the model results show that the front position does not advance continuously in the horizontal direction, but it moves back and forth during the surface wave cycle, being influenced by the orbital velocity. In particular, during the interval from the passage of the crest (phase equal to 0) to the trough phase (π) the front is advected forward, while in the interval ($\pi - 2\pi$) the front is quasi-static, with a very small backward retreat. Then, during the following stages the front starts to advance again. In particular, the forward front velocities are larger between 0 and $\pi/2$. Since the horizontal orbital wave velocity is in phase with the surface elevation, they are positive in the interval $(-\pi/2 - \pi/2)$ and negative in the interval $(\pi/2 - 3\pi/2)$. It may be observed that there is a lag of about $\pi/2$ between the wave induced orbital velocity and the velocity of the pulsating front of the salt wedge, which may due to inertial effects.

Moreover, several oscillations of the front shape in the rear part of the lobe are observed in the experimental data. They can be related to the wave induced orbital velocity, which interacts with the K-H billows generated in the shear layer between the two fluids. The

model is able to reproduce such oscillations, although the predicted amplitude is smaller and their wavelength is larger, as it should be expected when considering 2D simulations (Ooi et al. 2009).

ENTRAINMENT

On the basis of numerical model results, the entrainment coefficient $E = w_e/(U - U_l)$ has been estimated, where U end U_l are the average velocity of the heavy and light front, moving onshore and offshore respectively; w_e is the bulk velocity of ambient fluid entering into the mass of the heavy fluid. The latter variable is estimated on the basis of the volume V of ambient fluid entrained into the heavy fluid. In particular w_e is obtained as the ratio between V and the product of the time t, the width of the flume and the length of the interface between the two fluids.

Figure 17 shows the entrainment coefficient E as function of the dimensionless time t^* for each simulated test. It is possible to note that the entrainment of the ambient fluid into the density current decreases over the time. Such a reduction is most important up to $t^* = 8$, after that the entrainment becomes more stable. The presence of waves (runs W004, W007, W008 and W009) causes an increase of entrainment near of about 20% with respect to the runs executed in the absence of surface waves (runs S004, S007, S008 and S009).

The entrainment coefficient E at the end of the numerical runs (for $t^* = 10$) is shown in Figure 18, as a function of the Froude number F. The numerical results, both in the absence an in the presence of surface waves, are superimposed with empirical formulations (Parker et al. 1987; Ross et al. 2006; Adduce et al. 2012) and with field data (Princevac et al. 2005). Since the numerical simulations have Reynolds number (Re) greater than 10^3, the tests do not match well with the formula of Parker et al. (1987), derived from tests carried out with $Re < 10^3$. Such differences can be related also to the high released volume, as found by Theiler and Franca (2016) in their experiments with a variable volume of the lock exchange. On the contrary the obtained results fit well with the formula of Adduce et al. (2012), derived for higher Reynolds numbers. Similar results have been also obtained by

means of field measurements in Princevac et al. (2005).

CONCLUSIONS

The effect of the superposition of surface regular waves on the propagation of gravity currents has been investigated both experimentally and numerically. A full-depth lock exchange configuration has been chosen because it allows to quickly reach a steady-state gravity current conditions, which has been extensively investigated in the past in the absence of superimposed surface gravity waves.

The present experimental investigation has been carried out in a wave flume, where the lock has been obtained by means of a removable gate located at the center of the flume. Both tests in the absence and in the presence of a regular surface wave field have been performed, by considering Boussinesq gravity currents, i.e. in a small range of reduced gravity values ($g' = 0.010 \div 0.172$ m/s^2). Reynolds numbers of the experiments, related to the average front velocity, were between 1500 and 20000. Linear regular surface waves have been generated and all the tests have been run in intermediate water depth conditions.

A new 2D numerical approach for modelling the combined gravity current-surface wave flow has been proposed. Assuming that at leading order the orbital motion is not affected by the Boussinesq current, a Boussinesq- type of model for wave propagation in non-stratified flow and a gravity current model for the stratified flow are coupled together. The gravity current velocities are defined as the difference between total and wave-induced orbital velocity. They are related to density variability in space and are evaluated by solving the density transport equation along with the RANS equations, with a Smagorinsky-type turbulence closure. Compared to previous numerical modelling techniques, such an approach is at the same time accurate, computationally efficient and able to catch some of the main features of the flow.

It is observed that in the present work the modification of the average front velocity in the presence of the waves is related just to the Stokes drift, i.e. to the component of the wave mass transport due to the irrotational motion. Indeed, only such a component of the

wave steady current is present, as the one due to the wave boundary layer dynamics is not developed due to the characteristics of the present experimental and numerical tests. Since in the present work only one wave condition was generated, the Stokes drift is constant throughout all the tests.

While the experimental results obtained without waves agree with the results previously obtained in the literature, the presence of the waves affects the gravity current propagation in several ways, which may significantly influence the capability of the current to trigger the transport materials, such as sediments or contaminants close the coast. In particular, compared to the case of pure buoyancy-driven flows:

- the Froude number of the gravity current F, and in turn the average front velocity U, may be decreased as a function of the relative importance of the Stokes drift compared to buoyancy;
- the shape of the advancing front is modified, with a less steep lobe and height of the rear part smaller than the value $h = H/2$ predicted by the energy conserving Benjamin's theory in the absence of waves;
- the dynamics of the heavy front shows a pulsating behavior, as it moves back and forth with the same oscillating period of the superimposed regular wave field;
- the instantaneous maximum velocity of the front can be increased up to 4 times with respect to the average one;
- the development of K-H billows at the interface between the heavy and the light fluids is affected by the presence of the waves, while small-scale turbulence may be damped due to the orbital motion, if the waves are in the laminar regime and the flow is wave-dominated.

The validation of the proposed numerical model has been carried out by using the present experimental dataset. The numerical front position is estimated by using the dimensionless density difference $\Delta\rho^*$, which ranges between 0 and 1, corresponding to the minimum and

783 the maximum density respectively. Both in the absence and in the presence of the superim-
784 posed surface waves, the agreement between experimental and numerical results is generally
785 reasonable, notwithstanding some differences observed during the initial transient after the
786 removal of the lock. In particular:

787 • the comparison between model and experiments in terms of front position highlights
788 that the use of $\Delta\rho^* = 0.125$ gives a better agreement with respect to larger values of
789 the relative density;
790 • the shape and the average velocity of the gravity current are well reproduced by the
791 numerical model, with the formation of a characteristic lobe on the more advanced
792 part of the current and of vortex structures at the interfaces between the two fluids;
793 • both the measured and calculated spectral components of the front position show that
794 the highest peak always appears in the correspondence of the monochromatic wave
795 frequency;
796 • a secondary peak is present at a lower frequency, probably due to long waves generated
797 by the initial opening of the gate;
798 • the width of the spectrum is proportional to the value of g', probably because of the
799 larger momentum exchange and of a greater instability of the shear layer;
800 • the presence of the waves causes an increase of about 20 % of the entrainment of
801 ambient fluid into the density current.

802 An intra-wave analysis has been carried out, which has further confirmed the ability of
803 the model to reproduce the wave-induced pulsating forward movement of the heavier front.
804 In summary, both the experimental and the numerical results show that, in estuarine and
805 nearshore regions, the effects of the wave oscillating motion on the propagation of gravity
806 current is significant. Indeed, on the one hand it may increase entrainment of ambient fluid
807 into density current, on the other hand it may slow down the current, at the same time
808 enhancing its transport and erosive potential, as a consequence of the wave-induced front

oscillations.

Future development of the present investigations includes: (i) from the experimental viewpoint, a systematic work to assess the effects of short and long waves on gravity current propagation; (ii) from the numerical viewpoint, an improvement of the turbulence closure in order to take into account the different scale of turbulence associated to the movement of the salt wedge.

ACKNOWLEDGEMENT

This work has been partly funded by the Italian Ministry of Education, Universities and Research MIUR through the Research projects of significant national interest - PRIN 2010-2011 - project name HYDROCAR (cod. $20104J2Y8M\_003$) and PRIN 2012 - project name "Hydro-morphodynamics modelling of coastal processes for engineering purposed" (cod. $2012BYTPR5$) and through the EU funded project HYDRALAB PLUS (proposal number 654110).

The authors would like to acknowledge the two anonymous reviewers, whose comments allowed to improve the quality of the paper.

REFERENCES

Adduce, C., Sciortino, G., and Proietti, S. (2012). "Gravity currents produced by lock exchanges: Experiments and simulations with a two-layer shallow-water model with entrainment." *Journal of Hydraulic Engineering*, 138(2), 111–121.

Benjamin, T. B. (1968). "Gravity currents and related phenomena." *J. Fluid Mech.*, 31(2), 209–248.

Crossland, C. J., Kremer, H. H., Lindeboom, H., Crossland, J. I. M., and Le Tissier, M. D. (2005). *Coastal fluxes in the Anthropocene: the land-ocean interactions in the coastal zone project of the International Geosphere-Biosphere Programme*. Springer Science & Business Media.

Dean, R. and Dalrymple, R. (1991). *Water wave mechanics for engineers and scientists*. World Scientific, Singapore.

836 Deardorff, J. W. (1970). "A numerical study of three-dimensional turbulent channel flow at
837 large reynolds numbers." *Journal of Fluid Mechanics*, 41, 453–480.
838 Goda, Y. and Suzuki, Y. (1976). "Estimation of incident and reflected waves in random
839 wave experiments." *Proceedings of 15th International Conference on Coastal Engineering*,
840 828–845.
841 Härtel, C., Carlsson, F., and Thunblom, M. (2000a). "Analysis and direct numerical simu-
842 lation of the flow at a gravity-current head. part 2. the lobe and cleft instability." *Journa*
843 *of Fluid Mechanics*, 418, 213–229.
844 Härtel, C., Meiburg, E., and Necker, F. (2000b). "Analysis and direct numerical simulation
845 of the flow at a gravity-current head. part 1. flow topology and front speed for slip and
846 no-slip boundaries.." *Journal of Fluid Mechanics*, 418, 189–212.
847 Huppert, H. E. and Simpson, J. E. (1980). "The slumping of gravity currents." *Journal of*
848 *Fluid Mechanics*, 99(4), 785–799.
849 Johnson, C. and Hogg, A. (2013). "Entraining gravity currents." *Journal Fluid Mechanics*,
850 731, 477–508.
851 Kolar, R., Kibbey, T., Sxpilka, C., Dresback, K., Tromble, E., Toohey, I., Hoggan, J.,
852 and Atkinson, J. (2009). "Process-oriented tests for validation of baroclinic shallow water
853 mmodel: the lock-exchange problem." *Ocean Modelling*, 28, 137–152.
854 La Rocca, M., Adduce, C., Lombardi, V., Sciortino, G., and Hinkelmann, R. (2012). "Devel-
855 opment of a Lattice Boltzmann method for two-layer shallow-water flow." *International*
856 *Journal for Numerical Methods in Fluids*, 70, 1048–1072.
857 La Rocca, M., Adduce, C., Sciortino, G., and Pinzon, A. B. (2008). "Experimental and
858 numerical simulation of the three-dimensional gravity currents on smooth and rough bot-
859 tom." *Physics of Fluids*, 20, 106603–1–106603–15.
860 Lo Re, C., Musumeci, R. E., and Foti, E. (2012). "A shoreline boundary condition for a
861 highly nonlinear boussinesq model for breaking waves." *Coastal Engineering*, 60, 41–52.
862 Lodhal, C., Sumer, B., and Fredse, J. (1998). "Turbulent combined oscillatory flow and

current in a pipe." *J. Fluid Mech.*, 373, 313–348.

Longuet-Higgins, M. S. (1970). "Longshore currents generated by obliquely incident sea waves, 1." *J. Geophys. Res.*, 75, 6778–6801.

Lowe, R., Rottman, J. W., and Linden, P. (2005). "The non-Boussinesq lock-exchange problem. part 1. theory and experiments." *Journa of Fluid Mechanics*, 537, 101–124.

Marino, B., Thomas, L., and Linden, P. (2005). "The front condition for gravity currents." *Journal of Fluid Mechanics*, 536, 49–78.

Mei, C., Stiassnie, M., and Yue, D.-P. (2005). *Theory and aapplication of ocean surface waves. Part 2: Nonlinear aspects*. World Scientific, Singapore.

Musumeci, R., Cavallaro, L., Foti, E., Scandura, P., and Blondeaux, P. (2006). "Waves plus currents crossing at right angle: experimental investigation." *Journal of Geophysical Research*, 111(C07019), 1–19.

Musumeci, R. E., Svendsen, I. A., and Veeramony, J. (2005). "The flow in the surf zone: a fully nonlinear boussinesq-type of approach." *Coastal Engineering*, 52, 565–598.

Ng, C.-O. and Fu, S.-C. (2002). "On the propagation of a two-dimensional viscous density current under surface waves." *Physics of Fluids*, 14(3), 970–984.

Nogueira, H., Adduce, C., Alves, E., and Franca, M. (2013). "Image analysis technique applied to lock-exchange gravity currents." *Measurement Science and Technology*, 24.

Nogueira, H. I. S., Adduce, C., Alves, E., and Franca, M. J. (2014). "Dynamics of the head of gravity currents." *Environmental Fluid Mechanics*, 14, 519–540.

Ooi, S., Constantinescu, G., and Weber, L. (2009). "Numerical ssimulation of lock-exchange compositional gravity current." *Journal of Fluid Mechanics*, 635, 361–388.

Ooi, S., Costantinescu, G., and Weber, L. (2007). "A numerical study of intrusive compositional gravity currents." *Physics of Fluids*, 19, 076602–1–076602–14.

Parker, G., Garcia, M., Fukushima, Y., and Yu, W. (1987). "Experiments on turbidity currents over an erodible bed." *Journal of Hydraulic Research*, 25(1), 123–147.

Piomelli, U., Moin, P., and Ferziger, J. H. (1988). "Model consistency in large eddy simula-

tion of turbulent channel flows." *Physics of Fluids*, 31(7), 1884–1891.

Press, W. H., Flannery, B. P., Teukolsky, S. A., and Vetterling, W. T. (1992). *Numerical recipes in Fortran (2nd ed.)*. Cambridge University Press.

Princevac, M., Fernando, H. J. S., and Whiteman, C. D. (2005). "Turbulent entrainment into natural gravity-driven flows." *J. Fluid Mech.*, 533, 59–268.

Robinson, T. O., Eames, I., and Simons, R. (2006). "The effect of wave action on gravity current." *Coastal Dynamics 2005*, 1–13.

Robinson, T. O., Eames, I., and Simons, R. (2013). "Dense gravity currents moving beneath progressive free-surface water waves." *J. Fluid Mech.*, 725, 588–610.

Ross, A., Dalziel, S., and Linden, P. (2006). "Axisymmetric gravity currents on a cone." *Journa of Fluid Mechanics*, 565, 227–253.

Shin, J. O., Dalziel, S. B., and Linden, P. F. (2004). "Gravity currents produced by lock-exchange." *J. Fluid Mech.*, 521, 1–34.

Simpson, J. (1997). *Gravity currents in the environment and the laboratory*. Cambridge University Press.

Smagorinsky, J. (1964). "Implications of dynamical modelling of the general circulation on long-range forecasting." *WMO-IUGG Symposium on Research and Development Aspects of Long-range Forecasting, WMO Technical Note 62*, 62, 131–137.

Svendsen, I. A., Madsen, P. A., and Hansen, J. B. (1978). "Wave characteristics in the surf zone." *Proc. 16th Coast. Eng. Conf.*, Vol. I (Chap. 29), Hamburg, 520–539.

Theiler, Q. and Franca, M. J. (2016). "Contained density currents with high volume of release." *Sedimentology*, 63(6), 1820–1842.

Turner, J. (1973). *Buoyancy effects in fluids*. Cambridge University Press.

Ungarish, M. (2007). "A shallow-water model for high-reynolds-number gravity currents for a wide range of density differences and fractional depths." *Journal of Fluid Mechanics*, 579, 373–382.

Ungarish, M. (2009). *An introduction to gravity currents and intrusions*. CRC Press Taylor

917 & Francis Group.

918 van Dongeren, A. R. and Svendsen, I. A. (1997). "Absorbing-generating boundary condition
919 for shallow water models." *J. of Waterway, Port, Coast. and Oc. Engnrg*, 123(6), 303–313.

920 Viviano, A., Musumeci, R. E., and Foti, E. (2014). "Boussinesq modelling of the impact of
921 pressure retarded osmosis plants in nearshore regions." *3rd IAHR Europe Congress, Book*
922 *of Proceedings*, Porto (Portugal) (April 14-16).

923 Viviano, A., Musumeci, R. E., and Foti, E. (2015). "A nonlinear rotational, quasi-2DH nu-
924 merical model for spilling wave propagation." *Applied Mathematical Modelling*, 39, 1099–
925 1118.

926 Viviano, A., Musumeci, R. E., and Foti, E. (2016). "Effect of surface waves on full depth
927 lock exchange gravity currents hydrodynamics." *River Flow 2016*, 848–854.

928 Wright, L., Friedrichs, C., Kim, S., and Scully, M. (2001). "Effects of ambient currents and
929 waves on graivty-driven sediment transport on continentaly shelves." *Marine Geology*,
930 (175), 25–45.

931 Wright, L. D., Wiseman, W. J., Bornhold, B. D., Prior, D. B., Suhayda, J. N., Keller, G. H.,
932 Yang, Z.-S., and Fan, Y. B. (1988). "Marine dispersal and deposition of Yellow River silts
933 by gravity-driven underflows." *Nature*, (332), 629–632.

List of Tables

TABLE 1. Control parameters of the experiments.

Test	h [m]	R [-]	ρ_0 [kg/m^3]	ρ_1 [kg/m^3]	γ [-]	g' [m/s^2]	T_w [s]	H_w [m]
S001	0.19	0.035	997.7366	999.0418	0.999	0.013	-	-
S002	0.18	0.033	997.7233	999.2565	0.998	0.015	-	-
S003	0.16	0.030	997.8030	999.7084	0.998	0.019	-	-
S004	0.20	0.036	997.8561	1000.0117	0.998	0.021	-	-
S005	0.17	0.030	997.8494	1001.2682	0.997	0.034	-	-
S006	0.16	0.029	997.7831	999.8046	0.998	0.020	-	-
S007	0.20	0.036	998.8566	1003.6741	0.995	0.047	-	-
S008	0.20	0.036	998.7556	1010.2907	0.989	0.113	-	-
S009	0.20	0.036	998.7050	1009.5909	0.989	0.107	-	-
W001	0.19	0.035	998.2409	999.7787	0.998	0.015	0.97	0.020
W002	0.18	0.033	998.2309	999.2564	0.999	0.010	1.00	0.018
W003	0.15	0.028	998.0220	999.1686	0.999	0.011	1.00	0.020
W004	0.20	0.036	998.1414	1000.5077	0.998	0.023	0.99	0.019
W005	0.17	0.030	997.9954	1001.1804	0.997	0.031	0.99	0.017
W006	0.17	0.030	997.7764	999.0104	0.999	0.012	0.99	0.017
W007	0.20	0.036	998.8566	1003.6894	0.995	0.047	0.99	0.019
W008	0.20	0.036	998.8567	1016.3537	0.983	0.172	0.99	0.019
W009	0.20	0.036	998.7050	1009.3792	0.989	0.105	0.99	0.019

TABLE 2. Comparison between the control parameters of the coupled experiments.

Coupled test	$e_{g'}$	e_{ub}	e_{Tc}
S001-W001	0.18	0.09	0.08
S002-W002	0.33	0.18	0.22
S003-W003	0.40	0.25	0.24
S004-W004	0.10	0.05	0.05
S005-W005	0.07	0.03	0.04
S006-W006	0.39	0.21	0.30
S007-W007	0.00	0.00	0.00
S008-W008	0.52	0.23	0.19
S009-W009	0.02	0.01	0.01

TABLE 3. Main parameters obtained from the performed experiments.

Test	U [m/s]	F [-]	Re [-]	kh [-]	ka [-]
S001	0.025	0.502	4712	-	-
S002	0.024	0.451	4230	-	-
S003	0.025	0.446	4051	-	-
S004	0.021	0.329	4280	-	-
S005	0.035	0.477	5858	-	-
S006	0.031	0.557	5024	-	-
S007	0.046	0.473	9200	-	-
S008	0.081	0.539	16220	-	-
S009	0.062	0.423	12380	-	-
W001	0.015	0.276	2812	1.049	0.0542
W002	0.016	0.373	2862	0.964	0.0495
W003	0.010	0.249	1566	0.875	0.0566
W004	0.015	0.227	3100	1.045	0.0505
W005	0.027	0.380	4505	0.928	0.0488
W006	0.021	0.469	3465	0.928	0.0488
W007	0.038	0.387	7540	1.045	0.0505
W008	0.094	0.507	18780	1.045	0.0505
W009	0.066	0.458	13260	1.045	0.0505

List of Figures

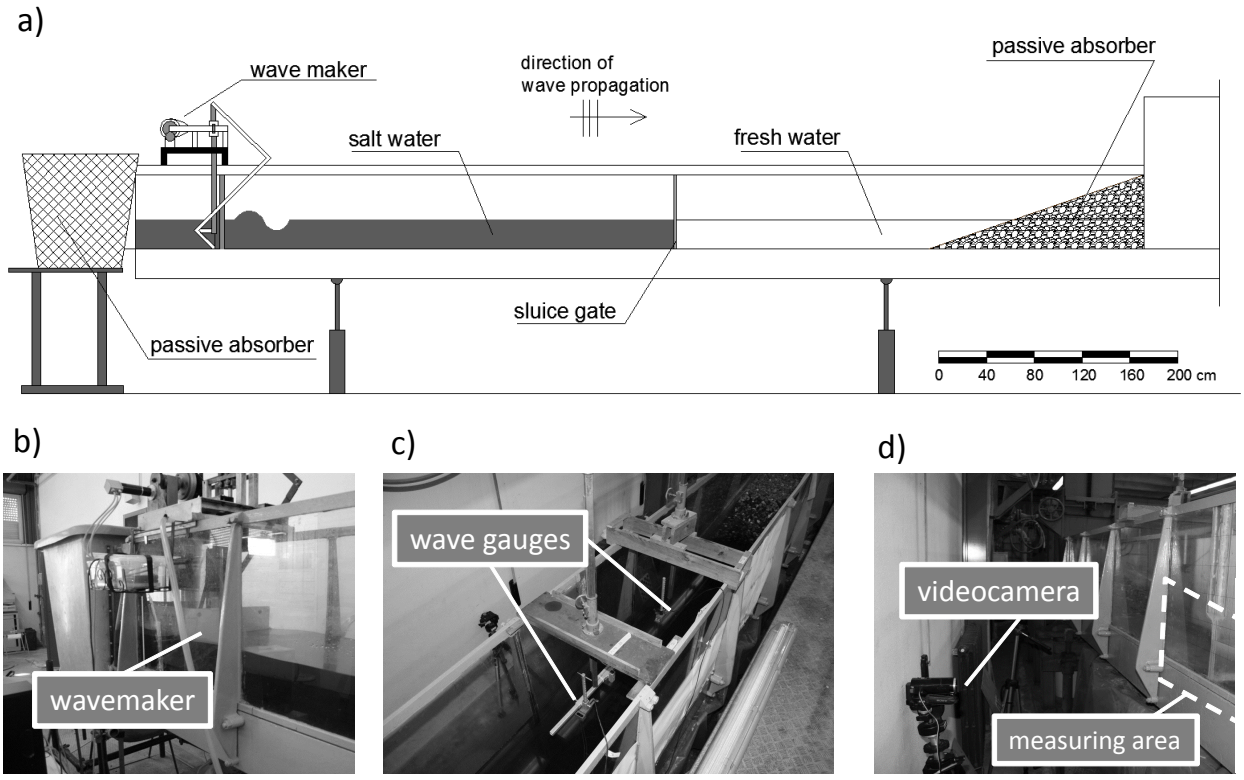

FIG. 1. a) Section of the experimental wave flume; b) Wavemaker at the offshore end of the flume; c) Resistive wave gauges used to measure wave parameters; d) CCD camera located in front of the measuring area.

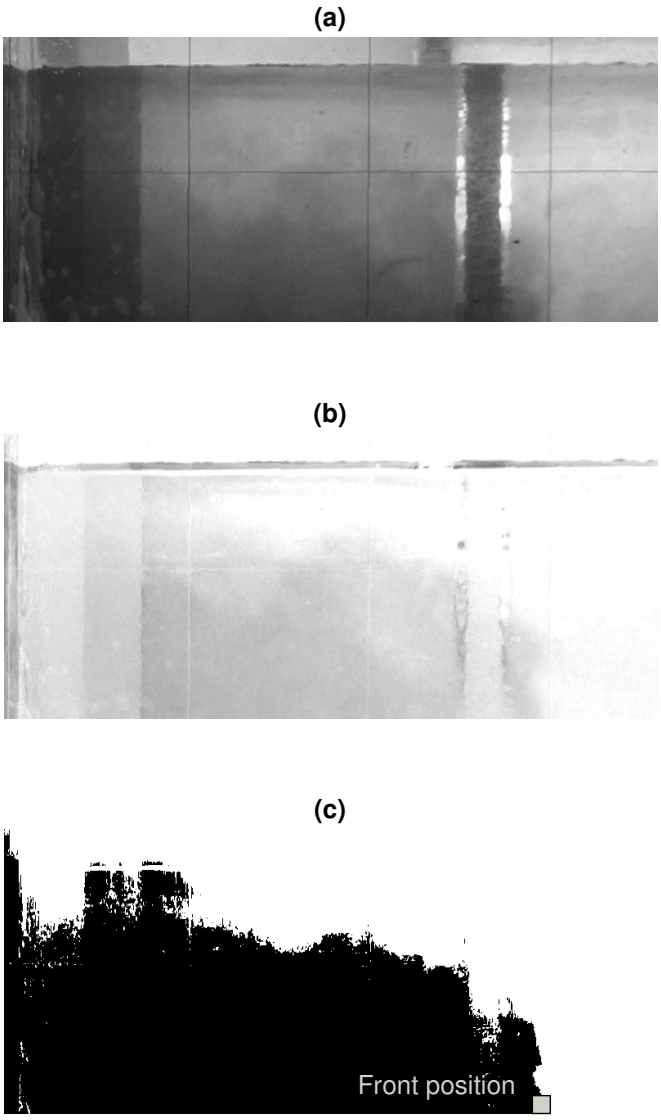

FIG. 2. Example of the image analysis procedure a) grayscale image converted from the original color image; b) enhanced grayscale image, obtained by subtracting the initial image from the actual one, in order to remove any influence of the initial condition; c) binary image used to detect automatically the shape and the position of the front of the gravity current.

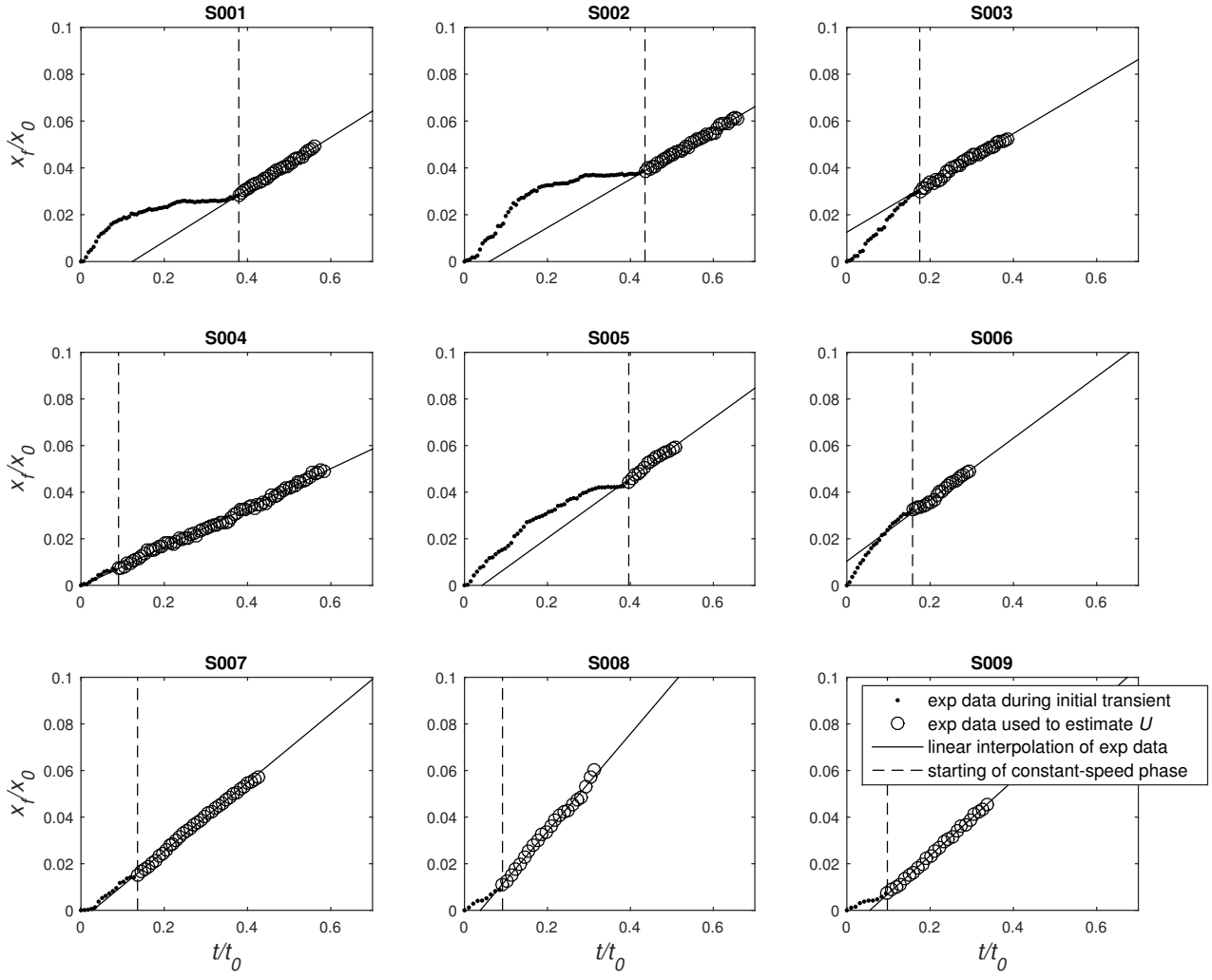

FIG. 3. Propagation of the position of the front of the gravity current in quiescent water conditions. Note that the acquisition frequency was 50 Hz, however here both sets of experimental data have been re-sampled at $f = 6.7$ Hz, in order to facilitate their graphical representation.

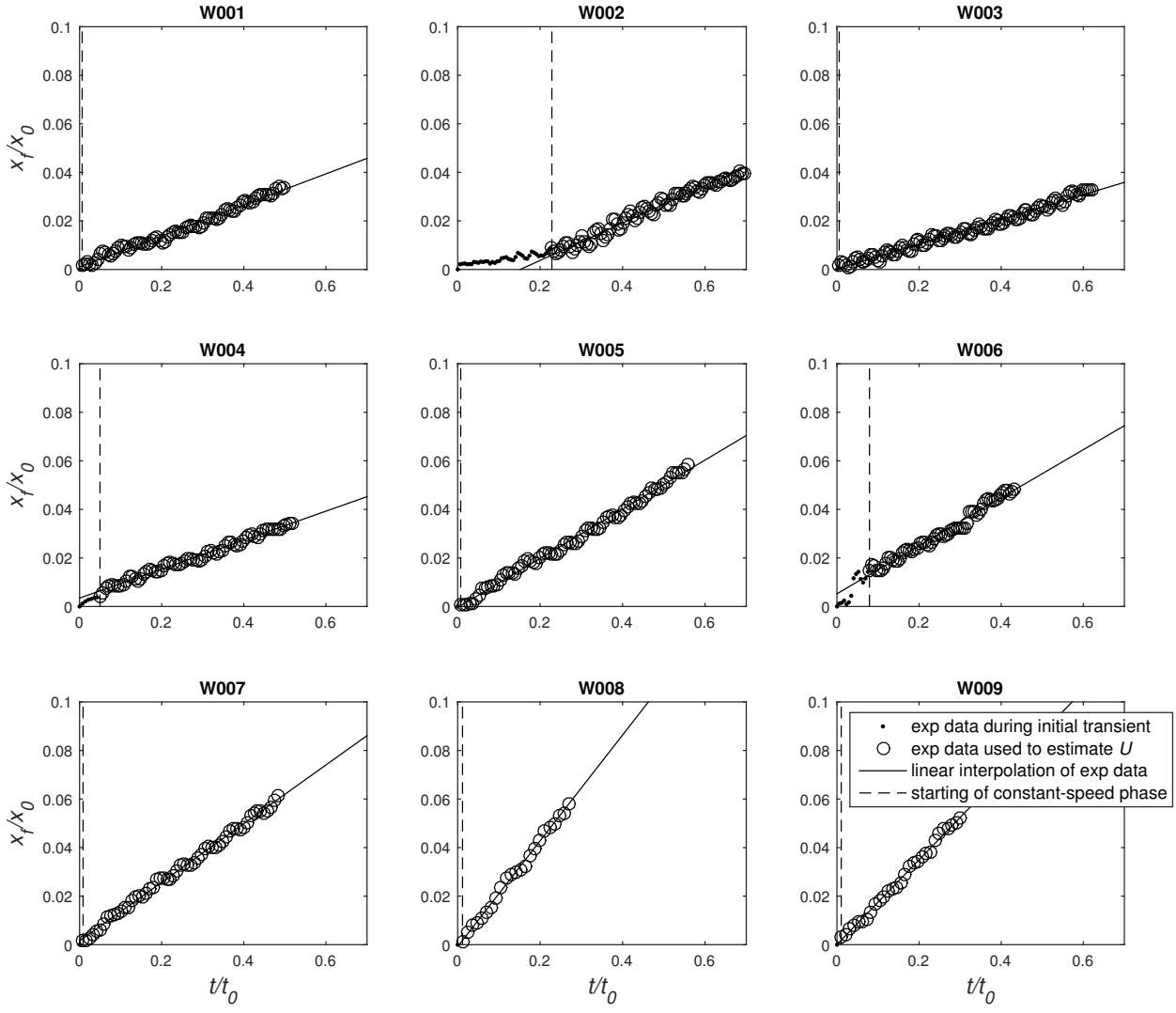

FIG. 4. Propagation of the position of the front of the gravity current in the presence of regular surface waves. Note that the acquisition frequency was 50 Hz, however here both sets of experimental data have been re-sampled at $f = 6.7$ Hz, in order to facilitate their graphical representation.

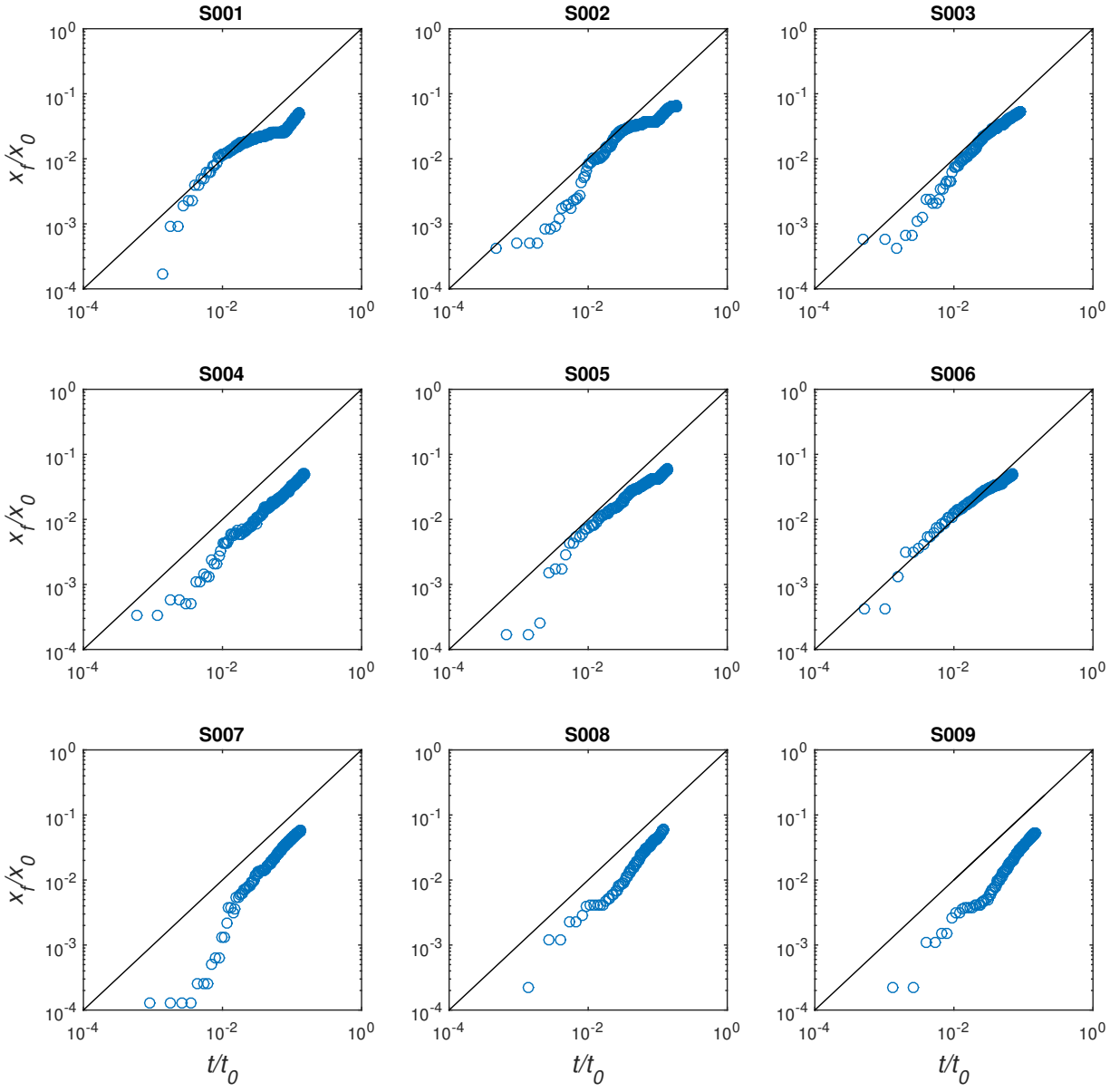

FIG. 5. Evolution of the non-dimensional front position $(x_f - x_0)/x_0$ with time t/t_0 on a log-log scale tests S001-S009, carried out in the ablsence of waves. The solid line represent the curve of the slumping stage, with slope equal to 1.

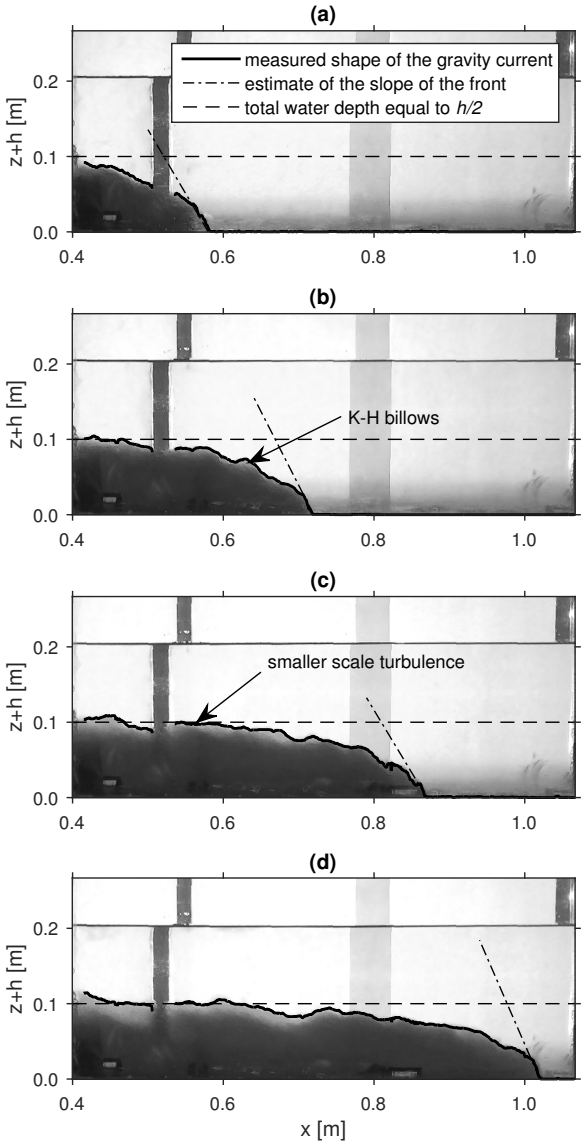

FIG. 6. Evolution of gravity currents in the absence of waves at different instants. (a) t=9s; (b) t=11s;(c) t=13s; (d) t=15s. The lock gate is located at x=0m (Experiment no. S008).

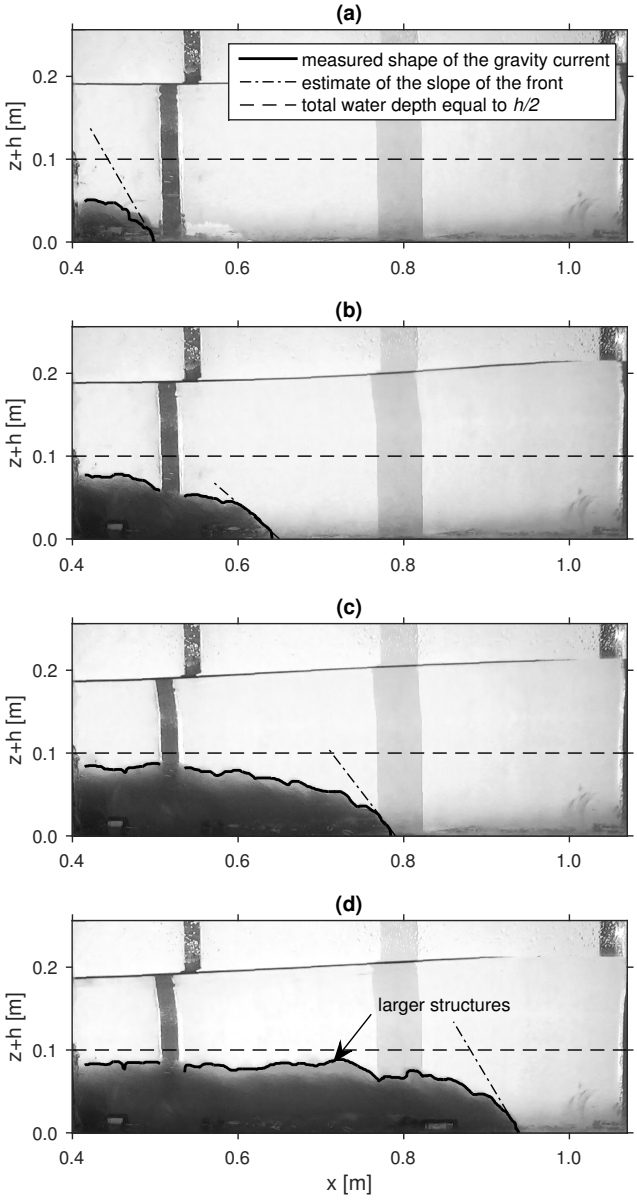

FIG. 7. Evolution of gravity currents in the presence of waves at different instants. (a) t=9s; (b) t=11s;(c) t=13s; (d) t=15s. The lock gate is located at x=0m (Experiment no. S008).

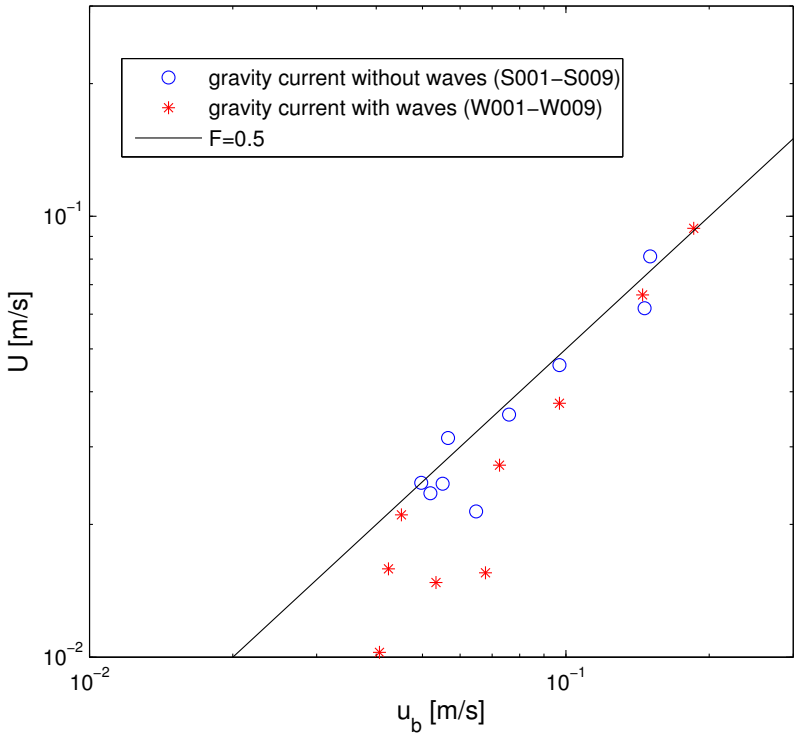

FIG. 8. Comparison between the measured average front velocity U and the buoyancy velocity $u_b = \sqrt{g'h}$ evaluated in term of the channel depth h in the presence and in the absence of waves. The solid line $F = 0.5$ corresponds to the theoretical prediction of the Froude number $F = U/u_b$ by the energy conserving theory of Benjamin (1968).

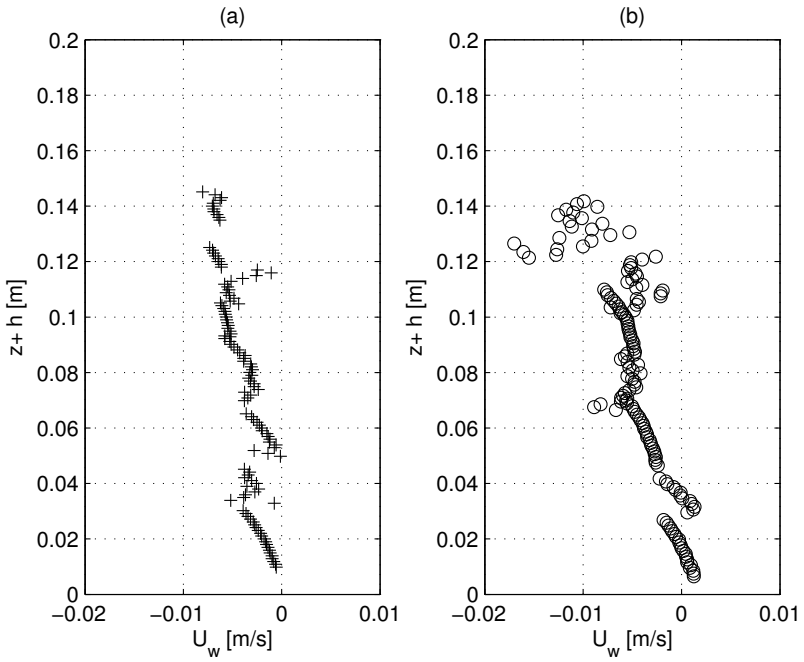

FIG. 9. Measure of the wave induced mass transport in terms of the time averaged velocity U_w along the water column, which has been estimated for different durations of the wave generation, i.e. about (a) 10s and (b) 60min.

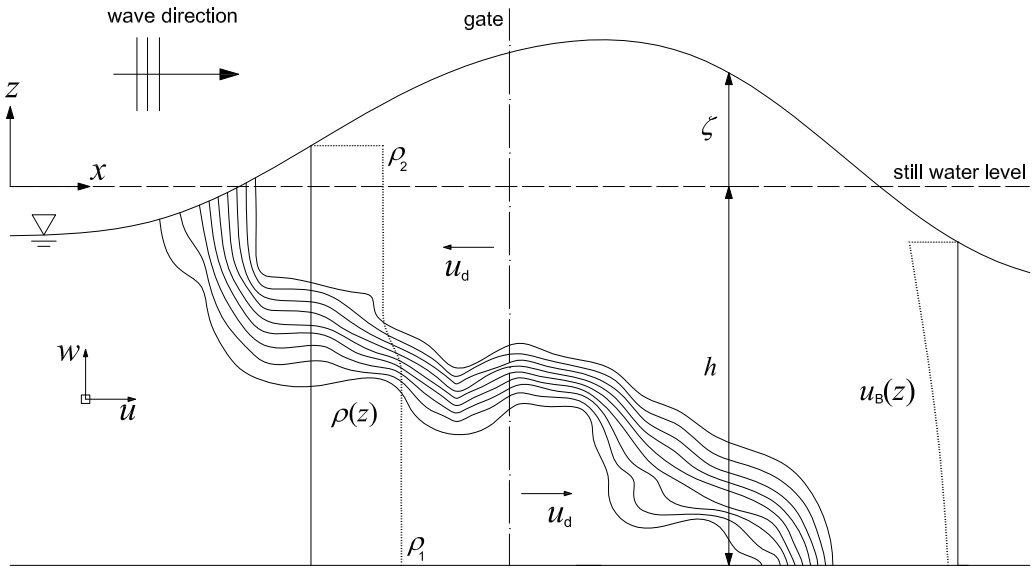

FIG. 10. Schematic description of the gravity current model for miscible fluids in the presence of surface waves.

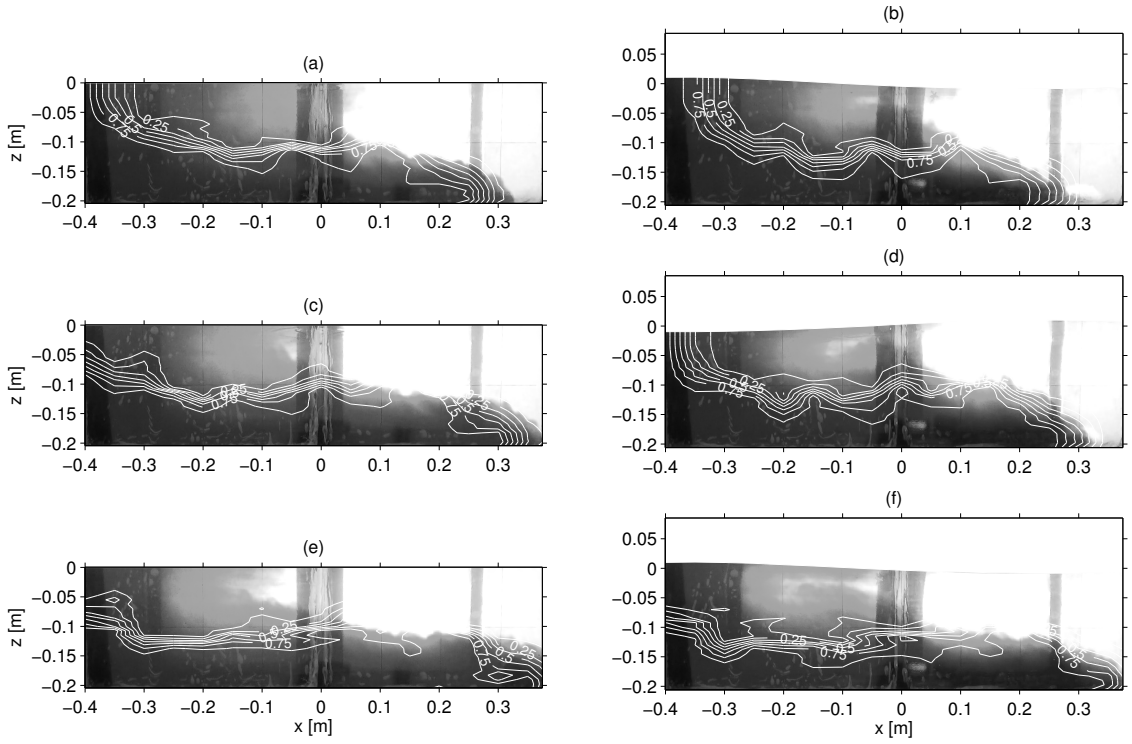

FIG. 11. Comparison between the evolution of the experimental front propagation (background image) and the calculated values of $\Delta\rho^*$ (isolines), both in the absence of waves (test S007) and in the presence of surfac waves (test W007). The position of the gate is located at $x = 0.0m$.(a) S007; $t = 7.5$ s; (b) W007; $t = 7.5$ s; (c) S007; $t = 9$ s; (d) W007; $t = 9$ s; (e) S007; $t = 10.5$ s; (f) W007; $t = 10.5$ s.

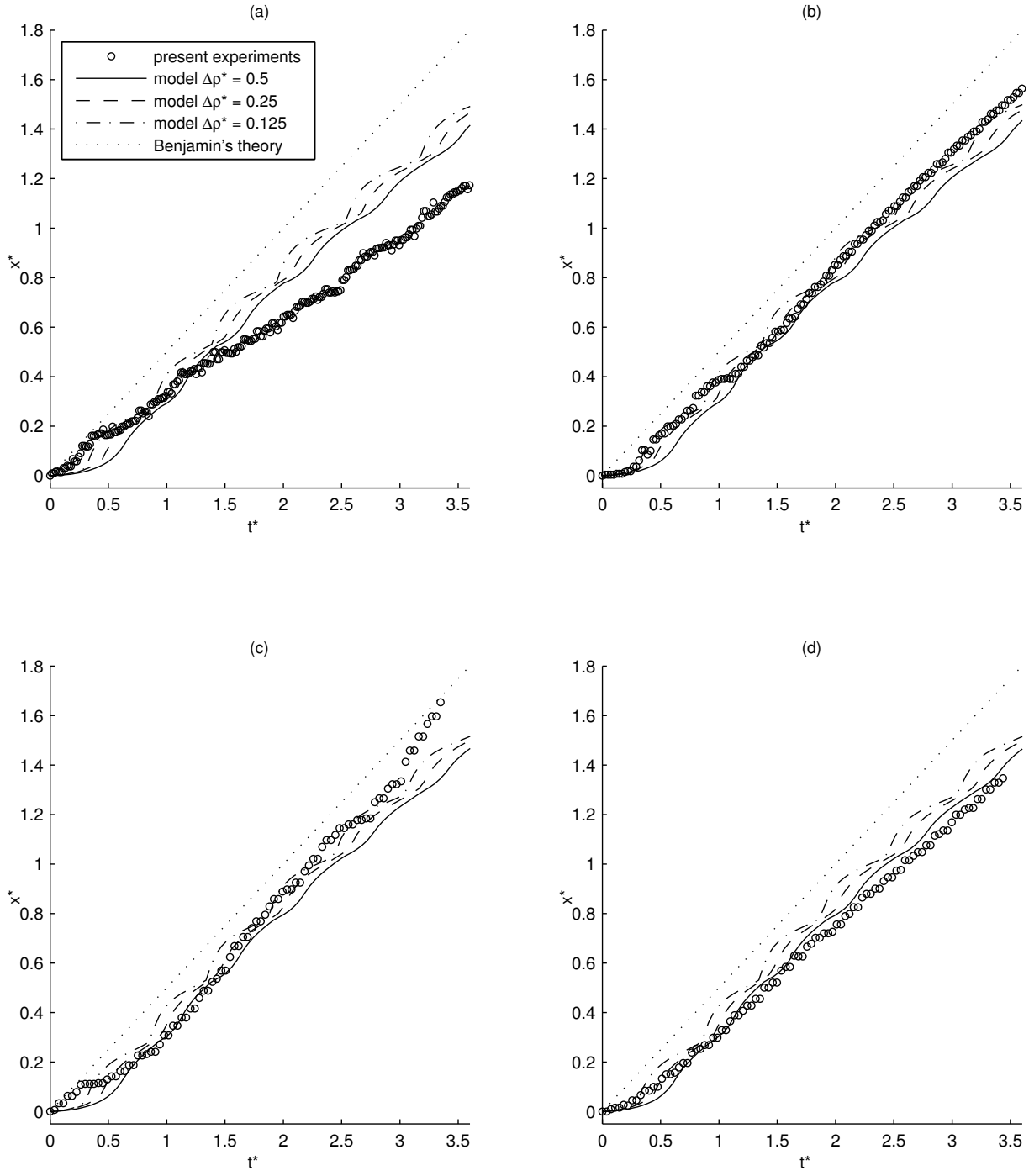

FIG. 12. Comparisons between the experimental time series of the heavy front position of the gravity current in the absence of waves (circles) in terms of the dimensionless time $t^* = t\sqrt{g'h}/h$ and position $x^* = x/h$ and that of the simulated front, calculated using $\Delta\rho^* = 0.125$, 0.25 and 0.5; the theoretical prediction of Benjamin(1969) is also plotted: (a) test S004, $g' = 0.021$ m/s^2; (b) test S007, $g' = 0.047$ m/s^2; (c) test S008, $g' = 0.113$ m/s^2; (d) test S009, $g' = 0.107$ m/s^2.

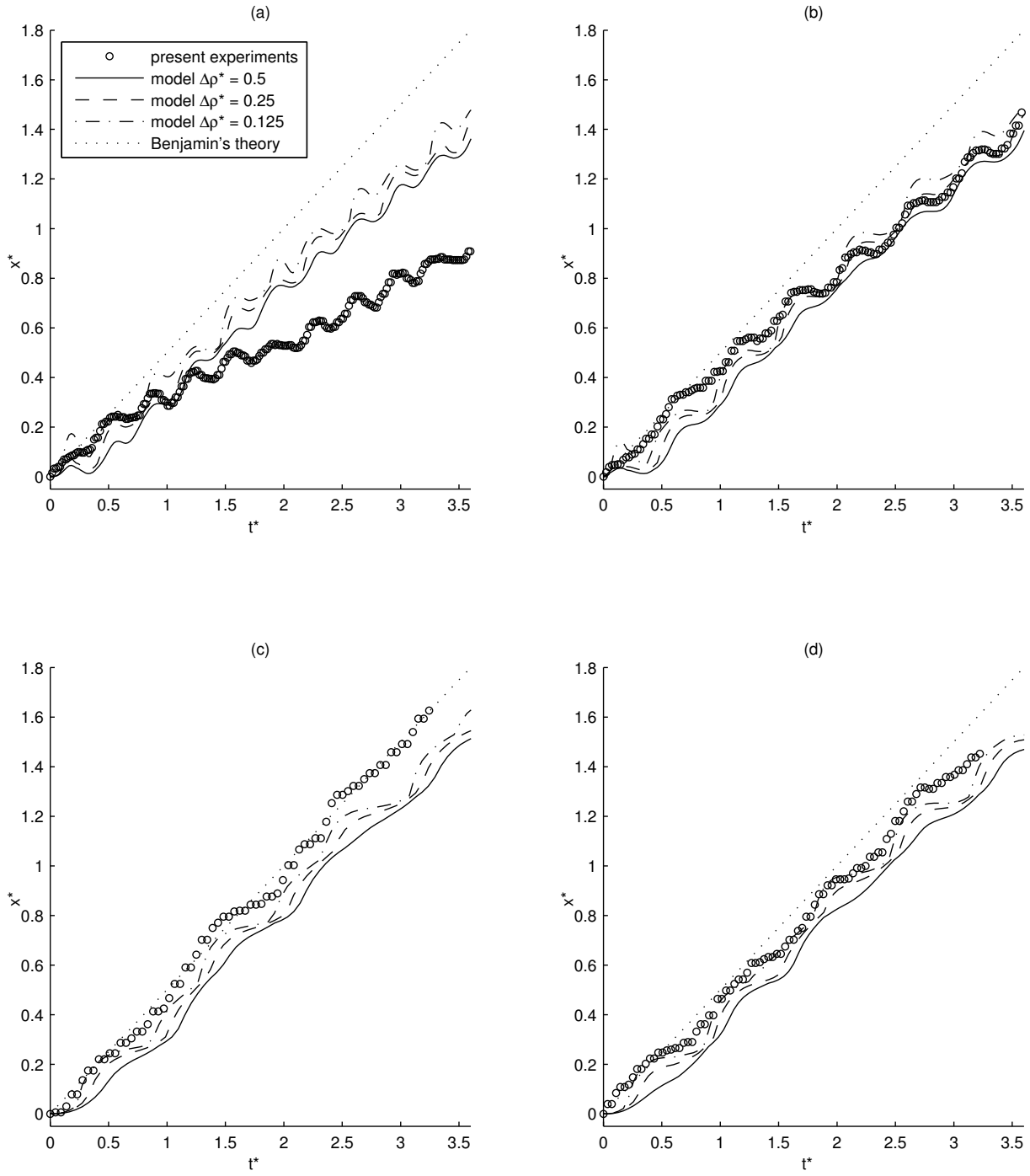

FIG. 13. Comparisons between the experimental time series of the heavy front position of the gravity current in the presence of waves (circles) in terms of the dimensionless time time $t^* = t\sqrt{g'h}/h$ and position $x^* = x/h$ and that of the simulated front, calculated using $\Delta\rho^* = 0.125$, 0.25 and 0.5; the theoretical prediction of Benjamin (1969) is also plotted: (a) test W004, $g' = 0.023$ m/s^2; (b) test W007, $g' = 0.047$ m/s^2; (c) test W008, $g' = 0.172$ m/s^2; (d) test W009, $g' = 0.105$ m/s^2.

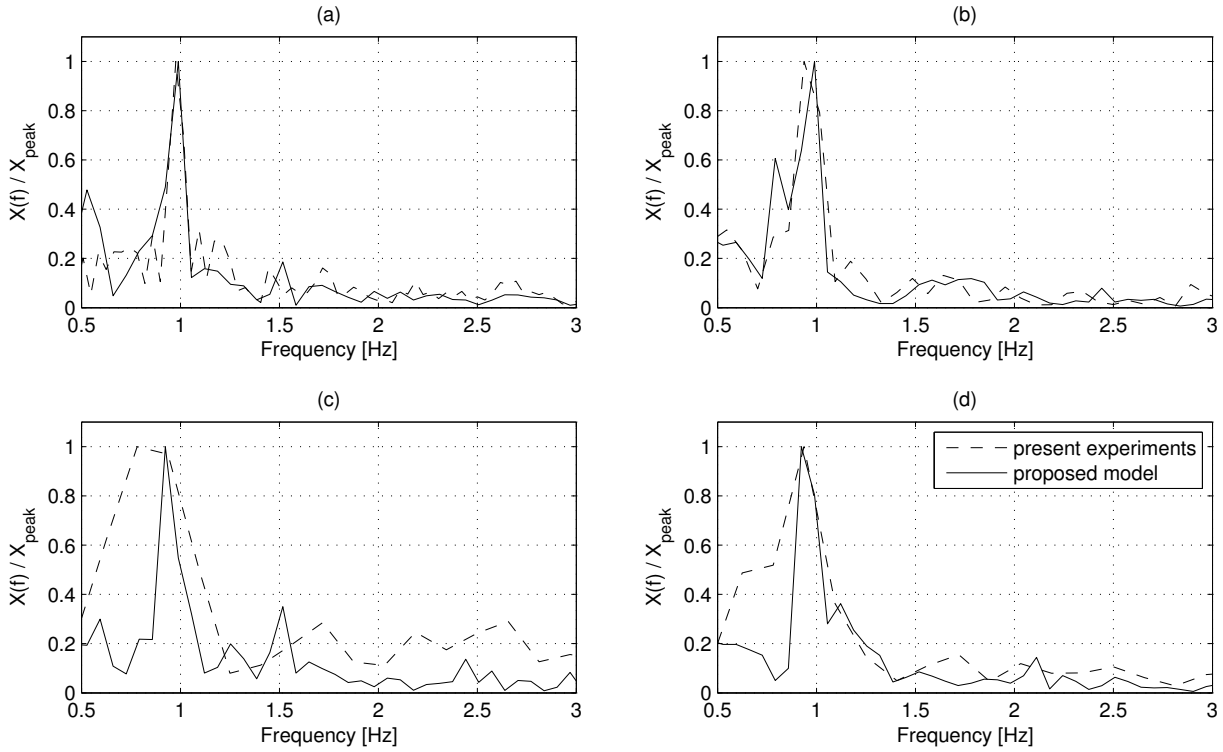

FIG. 14. Comparison between the normalized power spectra of the experimental and numerical front position signal, where the trend related to the current propagation has been removed. The front position has been calculated considering $\Delta\rho^* = 0.5$. Tests: (a) W004, $g' = 0.023$ m/s^2; (b) W007, $g' = 0.047$ m/s^2; (c) W008, $g' = 0.172$ m/s^2; (d) W009, $g' = 0.105$ m/s^2.

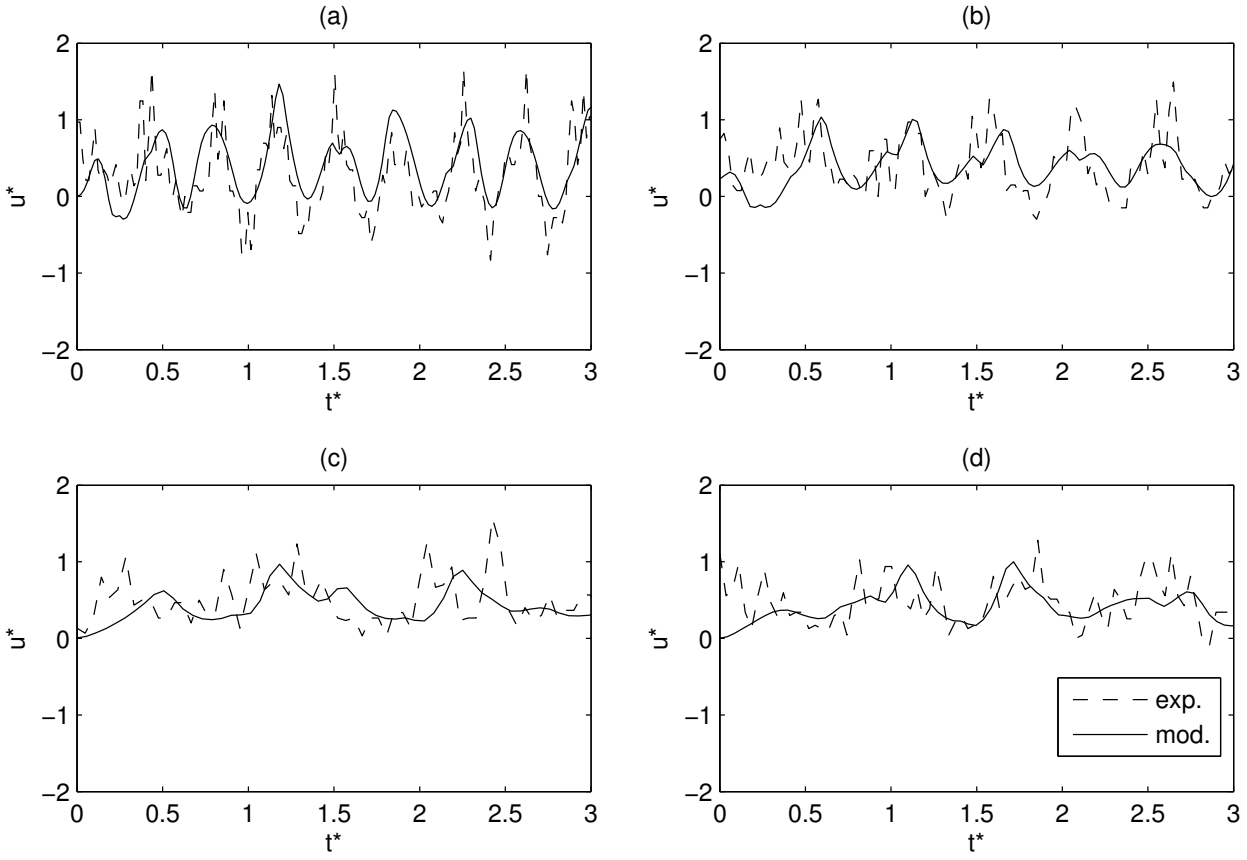

FIG. 15. Comparison between the measured and calculated instantaneous values of the dimensionless front velocity. The front position has been calculated considering $\Delta\rho^* = 0.5$. Tests: (a) W004, $g' = 0.023$ m/s^2, $T_w^* = 0.346$; (b) W007, $g' = 0.047$ m/s^2, $T_w^* = 0.495$; (c) W008, $g' = 0.172$ m/s^2, $T_w^* = 0.942$; (d) W009, $g' = 0.105$ m/s^2, $T_w^* = 0.735$.

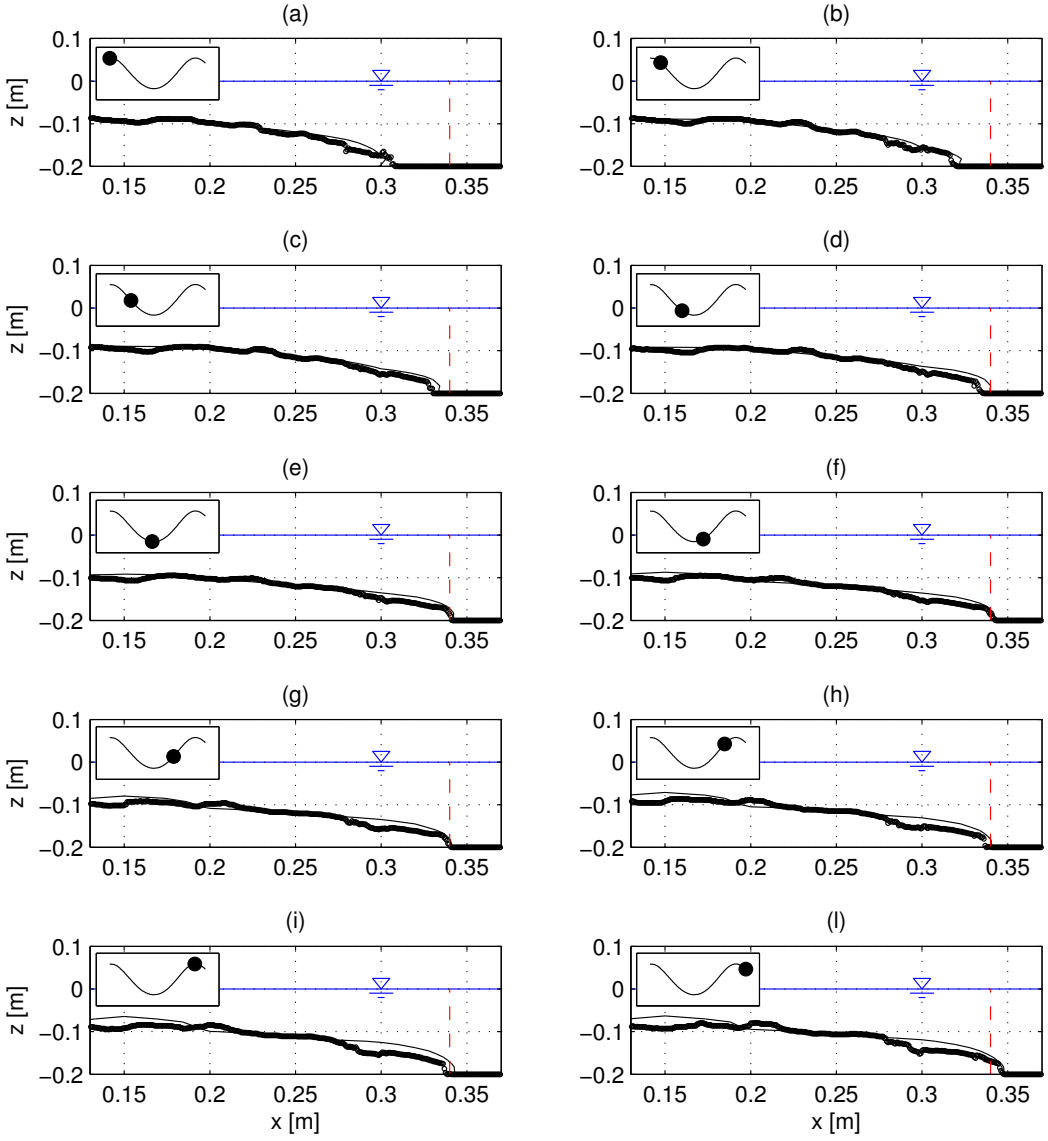

FIG. 16. Front propagation at several phases during the wave cycle: measured (dots) and calculated (solid line) front shape. The phase is assumed to be equal to zero when the wave crest reaches the front position. The modeled front is obtained by considering $\Delta\rho^* = 0.125$. Test W007 ($g' = 0.047$, $H_w = 0.019$, $T_w = 0.99s$ and $H = 0.20m$. The dashed line indicates a reference position at which the gravity current front is quasi-static. (a) phase = 0; (b) phase = $\pi/4$; (c) phase = $\pi/2$; (d) phase = $3\pi/4$; (e) phase = π; (f) phase = $5\pi/4$; (g) phase = $3\pi/2$; (h) phase = $7\pi/4$; (i) phase = 2π; (l) phase = $9\pi/4$.

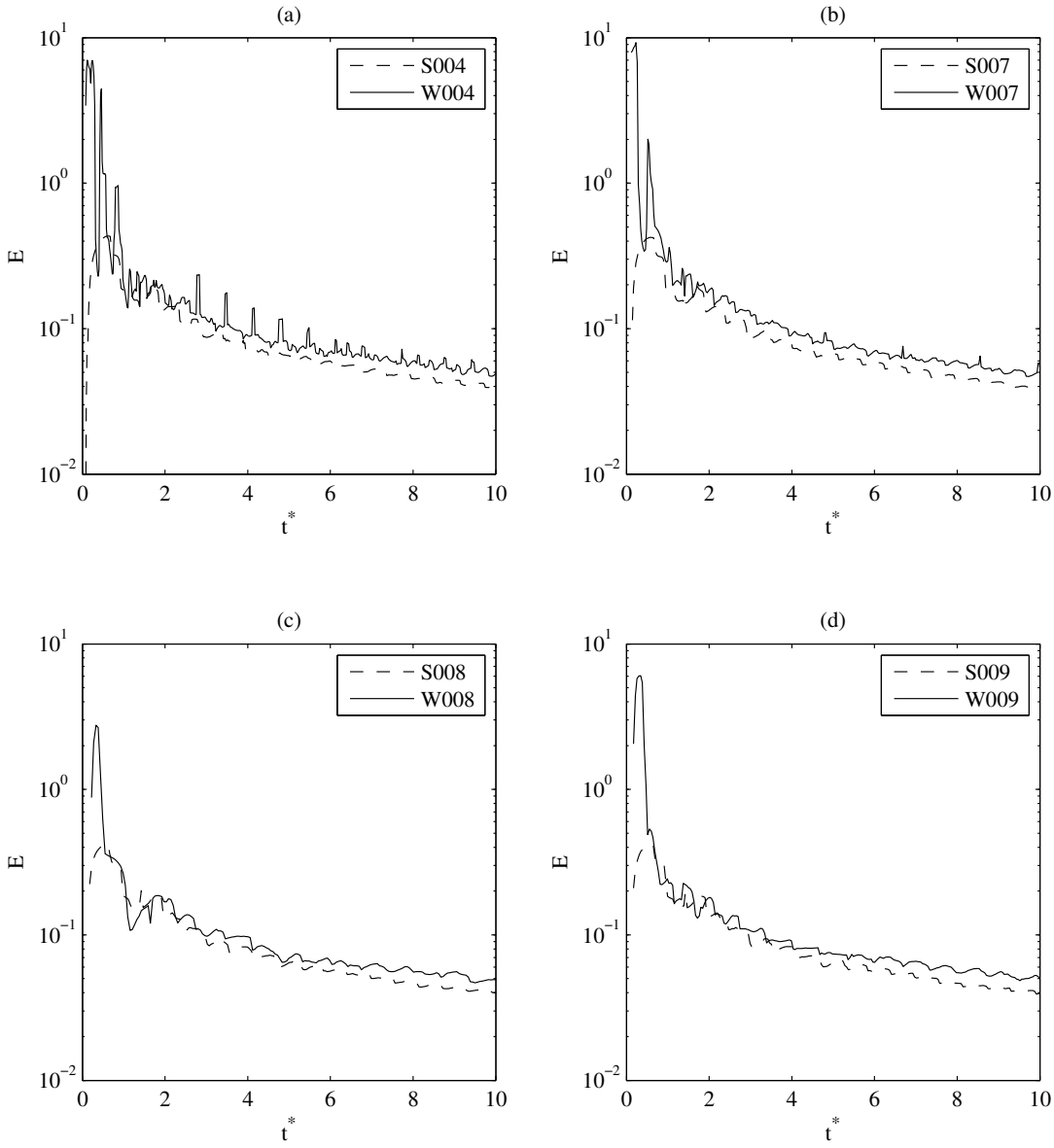

FIG. 17. Entrainment coefficient E from numerical model results as function of dimensionless time t^*: (a) tests S004 and W004; (b) tests S007 and W007; (c) tests S008 and W008; (d) tests S009 and W009.

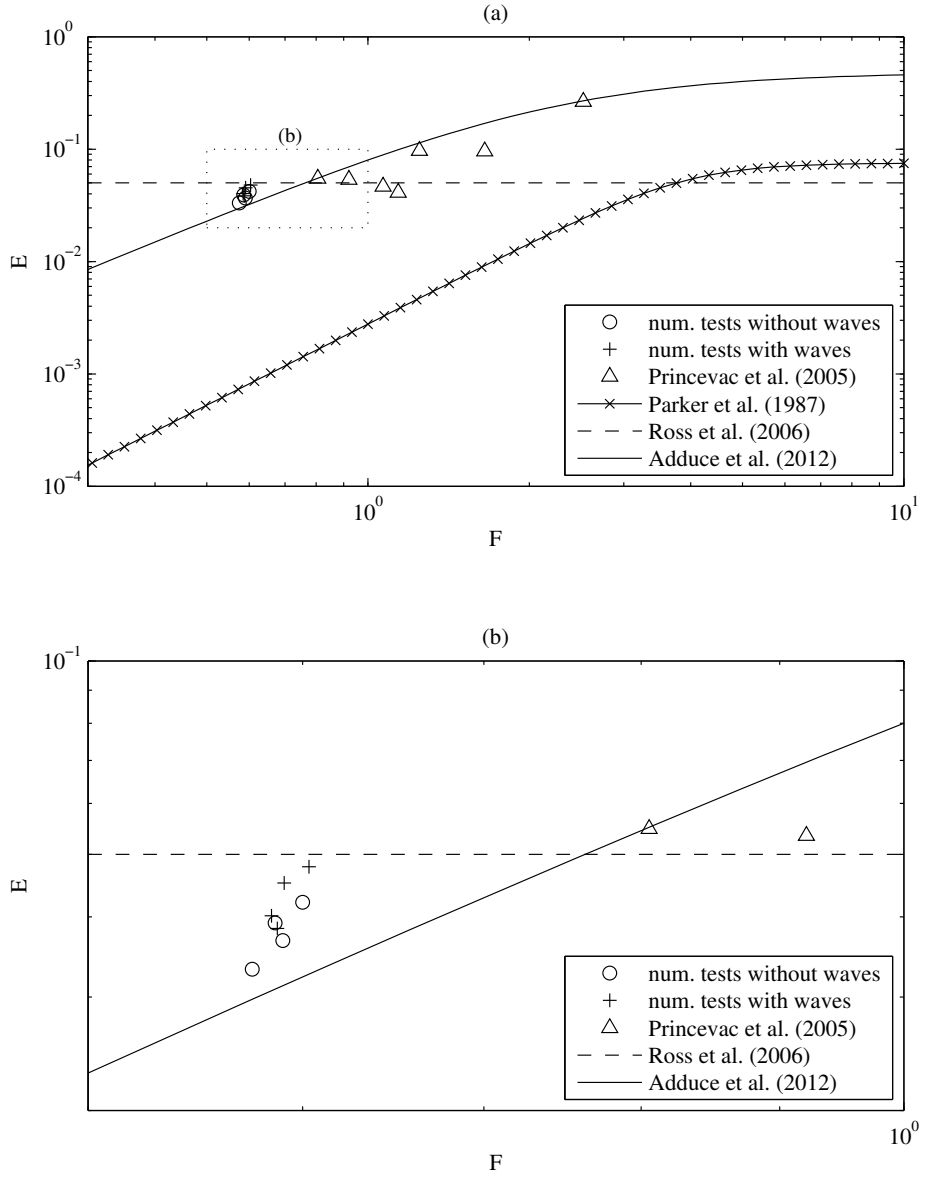

FIG. 18. Entrainment coefficient E at the end of numerical runs, i.e. for $t^* = 10$, as function of Froude number F; (a) comparison with field data (triangles) and synthetic formulations; (b) detailed view of the proposed numerical results.